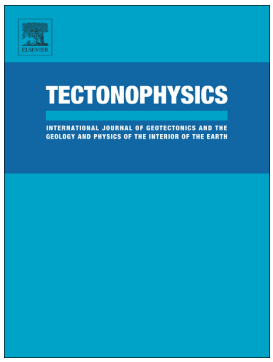

Dating the northern deposits of the Ebro foreland basin; implications for the kinematics of the SW Pyrenean front

B. Oliva-Urcia, E. Beamud, C. Arenas, E.L. Pueyo, M. Garcés, R. Soto, L. Valero, F.J. Pérez-Rivarés

PII: S0040-1951(19)30194-5
DOI: https://doi.org/10.1016/j.tecto.2019.05.007
Reference: TECTO 128113

To appear in: *Tectonophysics*

Received date: 30 December 2018
Revised date: 25 April 2019
Accepted date: 9 May 2019

Please cite this article as: B. Oliva-Urcia, E. Beamud, C. Arenas, et al., Dating the northern deposits of the Ebro foreland basin; implications for the kinematics of the SW Pyrenean front, Tectonophysics, https://doi.org/10.1016/j.tecto.2019.05.007

Dating the northern deposits of the Ebro foreland basin; implications for the kinematics of the SW Pyrenean front

Oliva-Urcia, B.[1,2,3]; Beamud, E.[4]; Arenas, C.[1,3]; Pueyo, E.L.[5]; Garcés. M.[6]; Soto, R[5]; Valero. L.[4,7]; Pérez-Rivarés, F.J.[1];

1. Dpto. de Ciencias de la Tierra. Universidad de Zaragoza. C/ Pedro Cerbuna 12. 50009 Zaragoza. Spain.
2. Dpto. de Geología y Geoquímica. Universidad Autónoma de Madrid. Ciudad Universitaria de Cantoblanco. 28049 Madrid. belen.oliva@uam.es
3. Geotransfer Group. Institute for Research on Environmental Sciences of Aragón (IUCA). University of Zaragoza. 50009 Zaragoza. Spain.
4. Laboratori de Paleomagnetisme CCiTUB-CSIC. Institut de Ciències de la Terra "Jaume Almera". C/ Solé i Sabarís s/n. 08028 Barcelona
5. Instituto Geológico y Minero de España. Unidad de Zaragoza. C/ Francisco Lasala 44. 9ºB. 50006 Zaragoza. Spain.
6. Departament de Dinàmica de La Terra i de l'Oceà. Universitat de Barcelona. C/Martí i Franquès s/n. 08028 Barcelona. Spain
7. Dpt. Geologia. Àrea d'Estratigrafia. Universitat Autònoma de Barcelona. C/ dels Til.lers. 08193 Bellaterra. Cerdanyola del Vallès. Barcelona.

Abstract

Dating the sedimentary infill of the northern margin of the Ebro foreland basin informs about the orogen-basin evolution. A magnetostratigraphic section of ~5 km-thick combines new magnetostratigraphic results from the syntectonic alluvial Uncastillo Fm (Upper Oligocene-Lower Miocene, 1 km-thick, the Fuencalderas section) with previous (3.3 km-thick) and new (0.7 km-thick) magnetostratigraphic data from the underlying fluvial Campodarbe Fm (Luesia and San Marzal sections, Eocene-Oligocene). This composite section allows dating the entire basin infill in this sector, therefore bracketing the timing of the deformation in the southern margin of the Pyrenees after considering previous kinematic studies. Deformation recorded by the continental deposits spans from syn-Gavarnie nappe activity (Broto and Fiscal basement thrust sheets) from 31.3 to 24.55 Ma, Rupelian-Chattian (Oligocene) to the syn-Guarga thrust activity, from 24.55 to 21.2 Ma Chattian-Aquitanian (Oligocene-Miocene). The Accumulation rates vary from ca. 22 to ca. 39 cm/kyr between the genetic stratigraphic units in the Uncastillo Fm through the section. These rates are close to those of the underlying deposits of the Campodarbe Fm (average of ca. 36 cm/kyr). Deformation for the latest Pyrenean front (syn-Guarga thrust) is younger than previously assigned in ~ 5.4. ~1.5 and ~1.1 Myr of the beginning of the Punta Común thrust sheet (from 29.4 Ma to 24 Ma), Lower Riglos thrust sheet system (from 24 to 22.5 Ma) and the Upper Riglos thrust system (22.5 to 21.4 Ma) respectively. Other significant changes in accumulation rate and its derivative also indicate variations in the tectonic activity ca. 33 and 28 Ma. Tilt variations in the Uncastillo Fm also record the tectonic activity with 40º variations of the Punta Común thrust sheet at ca. 20º with the Upper Riglos thrust sheet.

Key words: Magnetostratigraphy, dating, foreland basin, kinematics

1. Introduction

Foreland basins record the tectonic and denudation history of orogens (Jordan, 1981). The final architecture of the basin fill depends on the sediment supply from the eroding source region, the grain size distribution of that sediment supply, and the area available for sediment accumulation (Armitage et al., 2011; Heermance et al., 2007). Therefore, the final architecture of the basin fill relies on tectonic uplift-subsidence (Beaumont, 1981), the proximity of the sediment source to the depositional areas (Burbank and Beck, 1991), in addition to the type of the source rock lithology, e.g., how easily denuded or resistant to erosion is (Carroll et al., 2006). Consequently, the evolution of the foreland basins depends mainly on the tectonic uplift (generating relief prone to erode) and accommodation space, with the modulation by climate parameters, mainly runoff (Molnar, 2004).

To carry out the reconstruction of orogen-foreland basin evolution it is necessary to gather information about i) geometries and deformational history in the orogen, ii) architecture of the foreland basin fill (ages and sedimentary relationships/changes), iii) paleogeography of the foreland basin to determine the source area, iv) when available, cooling ages to assess denudation history, v) knowledge of the mechanical properties of foreland plate (DeCelles and Mitra, 1995; Schlunegger et al., 1997) and vi) paleoclimatic information (Molnar, 2004).

In the northern margin of the Ebro foreland basin, the six points mentioned above are relatively well known, and thus it is possible to reconstruct the orogen-continental foreland basin evolution: i) geometries and deformational history in the orogen (External Sierras, the frontal part of the basement unit uplifting the southern limit of the Pyrenees) are constrained thanks to stratigraphical and sedimentological studies by Millán-Garrido et al. (1995a), Millán-Garrido et al. (2000), Arenas et al. (2001) and Luzón (2005). In addition, the Ebro Basin has a fundamental chronostratigraphic frame based on increasing and extensive magnetostratigraphic studies (Burbank et al., 1992; Barberà et al., 1994; 2001; Gomis, 1997; Meigs, 1997; Gomis et al., 1999; Perez Rivarés et al., 2002; 2004; Larrasoaña et al., 2006; Costa et al., 2010; 2011; Valero et al., 2014). Except for some sections discussed in this paper (Hogan and Burbank, 1996; Oliva-Urcia et al., 2016), most of this large dataset is focused in the central parts of the basin. ii) The geometry and sedimentary evolution of the youngest sedimentary record, i.e. the architecture of the Luna fluvial system (Upper Oligocene-Lower Miocene), within the Uncastillo Fm, is well known (Arenas et al., 2001). The underlying fluvial deposits, i.e., the Campodarbe Fm, whose sedimentation was also influenced by the deformation history of the Pyrenean fold and thrust belt, has been also established

(Puigdefàbregas, 1975; Millán-Garrido et al., 1995a; Labaume et al., 2016). iii) The source areas of the Luna system include, from north to south: the Axial Zone, the Internal Sierras, the tubiditic and molasic deposits of the Jaca-Pamplona basin (Eocene-Oligocene basin north of the External Sierras), and the External Sierras of the Pyrenees (Arenas et al., 2001). To the east and to the north of the studied area, in the Huesca fluvial system, studies of sediment provenance allow constraining the geotectonic setting that controlled the foreland basin fill (Hirst and Nichols, 1986; Yuste et al., 2004; Roigé et al., 2016), iv) the source area ~100 km north was buried up to 4 km (Izquierdo-Llavall et al., 2013) and uplift ages from low temperature thermochronology data in the west-central Pyrenees reveal that exhumation occurred during the middle Eocene in the North-Pyrenean Zone, and migrated southward to reach the southern edge of the Axial Zone during the early Miocene (Labaume et al., 2016; Morris et al., 1998; Jolivet et al., 2007; and Bosch et al., 2016). v) The origin of the flexure of the lithosphere in relation to the tectonic activity has been discussed through time from i.e., the topographic load in the hinterland (Millán et al., 1995b) to subduction of the continental Iberian lithosphere (Gaspar-Escribano et al., 2001; Chevrot et al., 2014a; 2014b). In addition, the extension in the east from Late Oligocene to Neogene (opening of the Valencia trough) has also affected the uplift of the Ebro basin in its eastern part, conditioning the position of the depocenters in the Ebro basin (Gaspar-Escribano et al., 2001). vi) Climate in the Oligocene-Miocene has been extensively studied at global scale and orbital induced changes have been found (Zachos et al., 2001a; 2001b; Paul et al., 2010), as in the continental record of the central part of the Ebro basin (Luzón et al., 2002; Pérez-Rivarés et al., 2003. 2018; Valero et al., 2014). Compilations of stable isotope data ($\delta^{18}O$, $\delta^{13}C$) from marine sediments indicate Oi-1 and Mi-1 transient Antarctic glaciations at the Eocene-Oligocene and Oligocene-Miocene boundaries respectively, as well as an increase in temperatures at the end of the Oligocene (Late Oligocene Warming) (Zachos et al., 2001a; 2001b; Paul et al., 2000 and references therein). A summary of the climatic evolution of the Ebro basin during the Cenozoic has been collected in García-Castellanos et al. (2003) based on floral and faunal data. A warm to humid climate has been described for the Bartonian and warm to arid in the early Oligocene. During the late Miocene the climate became seasonal and humid (García-Castellanos et al., 2003 and references therein) and temperature slightly cooler (Vázquez-Urbez et al., 2013).

The contribution of this study is to provide new magnetostratigraphic data at the northern margin of the Ebro basin that, together with the previous Luesia 3300 m-thick section (Oliva-Urcia et al., 2016), allow better constraining: 1) the time framework for the deposition of alluvial and fluvial sediments in the entire northern margin of the Ebro foreland basin in this sector (ca. 5000 m-thick of basin infill), and 2) the timing of activity of the corresponding tectonic units in the southern front of the Pyrenees, comparing the new results with previous studies from the center of the Ebro basin

and with those from both, northern and southwestern margins (Hogan and Burbank, 1996; Larrasoaña et al., 2006; Oliva-Urcia et al., 2016; Perez-Rivarés et al., 2018) and kinematics in the Pyrenean Range (Labaume et al., 2016, Jolivet et al., 2007).

2. Geological setting

The Ebro Basin in NE Spain represents, at present, the latest evolutionary stage of the southern foreland basin of the Pyrenees, which formed as a result of the collision of the Iberian and Eurasian plates from Late Cretaceous to Miocene times. Earlier stages of the foreland basin are incorporated into the orogen (Jaca turbiditic and molasic piggy-back basins), on top of allochtonous thrust nappes (Ori and Friend, 1984; Puigdefàbregas et al., 1992) and they are involved in cannibalization, that is, the recycling of sediments within the sedimentary basin (Allen et al., 1986). The Ebro Basin was surrounded by active margins, the Pyrenees to the north, the Iberian Range to the south and the Catalan Coastal Ranges to the east (Fig. 1a), which efficiently supplied sediments to the basin. Sedimentary infill includes marine and continental sediments that range from late Cretaceous to middle-late Miocene in age. Marine connection persisted until the latest Eocene, ~ 36 Ma (Costa et al., 2010), when the basin was disconnected from the Atlantic Ocean and became fully endorheic (Riba et al., 1983; García-Castellanos et al., 2003). This reorganization favored the accumulation of several thousand meter-thick coarse to fine grained alluvial fluvial deposits along the margins and carbonate and evaporite lacustrine deposits towards the basin center. A complex history of progressive southwards and westward migration and compartmentalization of the depocenters of the foreland basin occurred linked to the evolution of the Pyrenean orogeny (Pérez et al., 1988; Muñoz et al., 2002; Valero et al., 2014). Thickness of the Paleogene-Neogene continental deposits range from 3580 m in the NW margin (Sangüesa well) to less than 300 m in the SE margin (Caspe well) as compiled in Zoetemeijer et al. (1990) based on IGME data (locations of wells in Fig. 1a). The South Pyrenean foreland basin was divided from Lutetian to early Miocene times into the piggyback Jaca–Pamplona Basin to the north and the present-day Ebro Basin to the south due to the development of the Gavarnie nappe in the External Sierras. In the west central southern Pyrenees, the External Sierras represent the southernmost outcropping thrust front in a foreland breaking sequence related to the Gavarnie nappe and Guarga basement thrust (Fig. 1a) (Puigdefàbregas, 1975; Labaume et al., 1985; Cámara and Klimowitz, 1985; McElroy, 1990; Pocoví et al., 1990; Millán-Garrido et al., 1995a; Teixell and García-Sansegundo, 1995; Millán-Garrido et al., 2000; Oliva-Urcia et al., 2012; Labaume and Teixell, 2018; Muñoz et al., 2018; Oliva-Urcia, 2018). More recently, the identification of new thrust faults in the Gavarnie nappe (or unit) near the study area has been published and the kinematic relationships between cover and basement thrust sheets based

on field geology and seismic profiles have been refined between middle Eocene to early Miocene (Labaume et al., 2016).

The studied Fuencalderas section is located at the northern margin of the Ebro foreland basin, south of the western sector of the External Sierras (Fig. 1b; 2a). The geological structure of the External Sierras, N of the Fuencalderas section, is the result of a hinterland imbricated thrust system younger from west to east and coeval with the early folding and later tightening of the detached WNW-ESE Santo Domingo anticline (Oligocene-Miocene) (Millán-Garrido et al., 1995a; 2000; Oliva-Urcia et al., 2012; Calvín et al., 2018 and references therein). The imbricated thrust sheet system is folded by, and crops out in, the southern limb of the Santo Domingo anticline (Fig. 2b). The thrust sheets are named, from west to east: Punta Común thrust sheet (PC), Lower Riglos thrust system (LRS), equivalent to Riglos thrust in Hogan and Burbank (1996), and Upper Riglos thrust system (URS), equivalent to Linás and Peña del Sol thrust sheets in Hogan and Burbank (1996) (Fig. 2a. 2b). Their lateral migration towards the east contrasts with the general previous progression of the deformation in the frontal thrust from east to west (Millán-Garrido et al., 1995a; 2000).

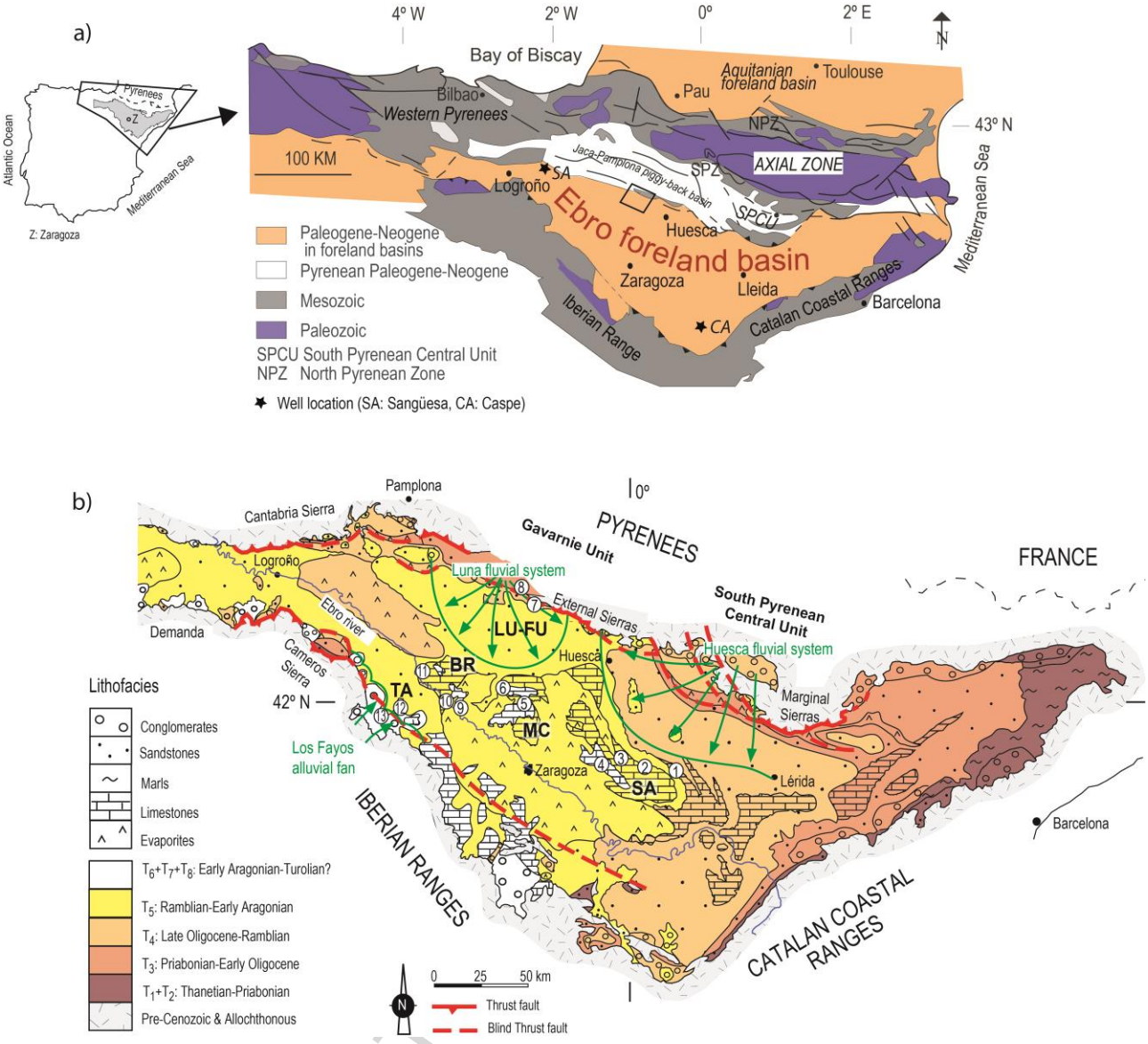

Fig. 1. a) Geological map of the NE of Spain. b) Map with tectosedimentary units (TSU) described in the Ebro Basin (adapted from Pardo et al., 2004). SA: Sierra de Alcubierre; MC: Montes de Castejón; BR: Bardenas; TA: Tarazona. Sections with magnetostratigraphic data: In SA. 1, Ontiñena; 2, Albalatillo; 3, Lanaja; 4, San Caprasio. In MC. 5, Esteban; 6, Sora (Pérez-Rivarés et al., 2018). In the Luna fluvial system: 7, Fuencalderas (this study); 8, Luesia (Oliva-Urcia et al., 2016) and this study; In BR. 9, Sancho Abarca; 10, Pico del Fraile; 11, Cabezo de Marijuán (Larrasoaña et al., 2006). In TA. 12, Lugar-Melero; 13, Umbría Alta (Pérez-Rivarés et al., 2018).

In the Ebro basin, eight tectosedimentary units[1] (TSU) have been described (Fig. 1b) (Muñoz et al.,

[1] A Tecto-Sedimentary Unit (TSU) is a "type of genetic stratigraphic unit made up of a succession of strata deposited within an interval of geological time and under a tectonic and sedimentary regime of definite polarity" (modified from Garrido-Megías, 1982). Its boundaries "have basinal extent and are generated by inflections or sharp changes in the rate of allocyclic factors that controlled basin fill dynamics (modified from Pardo et al., 1989 and Villena et al., 1996)", in Arenas et al. (2001).

2002). Dating of these units is based on fossil localities and magnetostratigraphic analyses (see compilation in Pardo et al., 2004 and Pérez-Rivarés et al., 2018). The latest syntectonic deposits in the northern west-central margin of the Ebro basin correspond to the Uncastillo Fm and the equivalent to the east to the Sariñena Formation (Quirantes, 1978), where units TSU 4 and 5 have been characterized (Arenas et al., 2001; Pardo et al., 2004; Luzón, 2005). Two large distributary fluvial systems with radial current distribution formed along the southern central Pyrenean margin (the Luna and the Huesca fluvial systems, Fig. 1b; Hirst and Nichols, 1986) existed during deposition of TSU 4 and 5, whose apices were separated ~100 km, and extended southward towards a lacustrine area in the center of the Basin. Numerous small alluvial fans coexisted with the large ones along that margin (Arenas et al., 2001; Luzón, 2005). The studied Fuencalderas section records the deposition of the medial-distal eastern sector of the Luna fluvial system, whose proximal sector was located approximately 8-10 km northwest of Fuencalderas section, to the north of the Luesia village (Figs. 2a. 3; Arenas et al., 2001). Three local stratigraphic genetic units were characterized in this system and correlated to basinal TSU 4 and 5 recognized through the rest of the basin (Figs. 2a. 3). The occurrence and sedimentary evolution of both the large and the concurrent small fans in the Luna system were related to the Gavarnie nappe activity and, particularly with the Guarga basement thrust sheet, which is associated with formation of the above mentioned thrust sheet system in the External Sierras: Punta Común thrust sheet (PC), Lower Riglos thrust system (LRS), and Upper Riglos thrust system (URS) (Arenas and Pardo, 1994; Arenas et al., 2001; Millán-Garrido et al., 1995a).

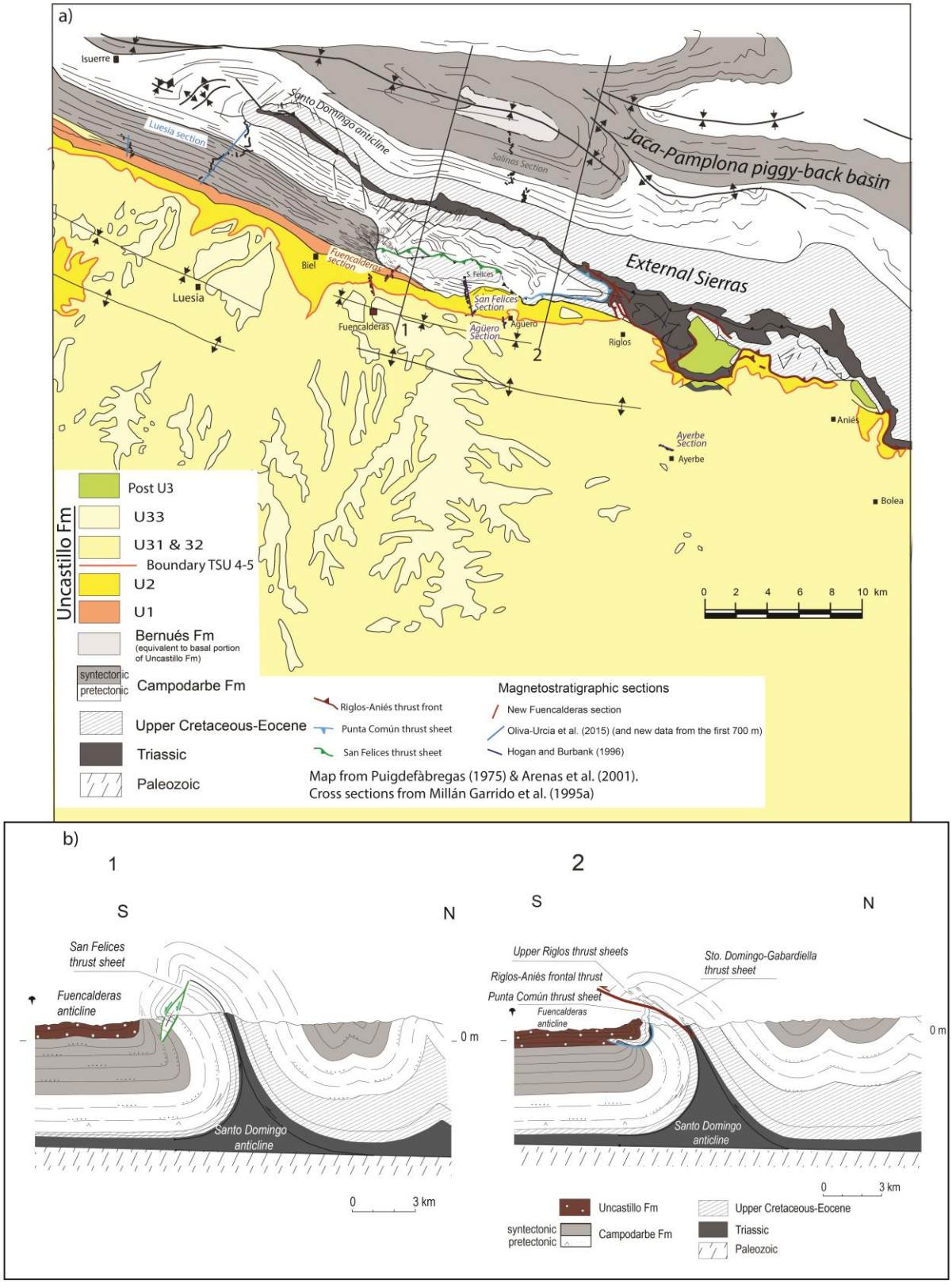

Fig. 2. a) Geological map of the studied area (modified from Puigdefàbregas, 1975; Arenas et al., 2001). Location of magnetostratigraphic sections are also shown. b) Cross sections of the External Sierras and thrust sheet system affecting the sediments of the northern margin of the Ebro foreland basin (Millán-Garrido et al., 1995a).

The Campodarbe Fm is divided into two units. The upper unit contains the syntectonic unconformity related to the San Felices thrust sheet (Gavarnie nappe) in the External Sierras (Puigdefàbregas, 1975) with an offlap-onlap "fan-shaped" geometry to the east and the correlative conformable strata to the west. The underlying Campodarbe strata represent the "pretectonic" unit (Puigdefàbregas, 1975; Millán-Garrido et al., 1995a; Oliva-Urcia et al., 2016).

The Luna system (Uncastillo Fm)

The sediment-source area for the Luna system includes the Jaca tubiditic and molasic basins, the Internal Sierras and further north, the Axial Zone. Most coarse sediments consist of sandstone grains from the Campodarbe Fm, and carbonate and minor siliceous grains from Mesozoic units in the Internal and External Sierras. The topographic variations of those source areas were related to the structural evolution of the Gavarnie nappe (Gavarnie, Broto and Fiscal-Guarga basement thrusts (Labaume et al., 2016). The source areas located around the Internal Sierras and south of the Axial Zone were buried ~ 4km after calculating P-T conditions by means of temperature-dependent clay mineral assemblages, vitrinite reflectance and fluid inclusion during burial that is, about 4 km of thickness were exhumed during the alpine orogeny after Rupelian times (Izquierdo-Llavall et al., 2013).

The deposits of the Luna system (TSU4 and 5) lie unconformably (angular unconformities) on Mesozoic and Cenozoic sedimentary units of the External Sierras, conforming several small alluvial fans (Fig. 2a). Local syntectonic unconformities are within unit 4 and between units 4 and 5 (Arenas et al., 2001). To the west, the equivalent TSU4 and 5 strata form a cumulative wedge-out system involving also the underlying sandstone and mudstone strata of the Campodarbe Fm (TSU3). The overall paleocurrent directions in the continental deposits changed from E-W to N-S in the Ebro Basin (Puigdefàbregas, 1975) at the end of the Campodarbe Fm in Chattian times (24.55 Ma) (Oliva-Urcia et al., 2016).

The Luna fluvial system is the result of the coalescence of two fluvial fans: Uncastillo to the west and Luesia to the east (Fig. 3). The deposits in the proximal and proximal-middle areas are conglomerates (having clasts well sorted and rounded, dominated by sandstone and less abundant carbonate grains) that change laterally to the medial and distal parts consisting of sandstones with variable amounts of mudstones, and locally limestones (Fig. 3). The small alluvial fans have rapid lateral facies changes between proximal and distal deposits, with limited development of the medial sectors. The conglomerates of the alluvial fans are composed of poorly sorted, angular and subrounded, dominant carbonate clasts derived from the External Sierras.

Three local tectosedimentary units (Uncastillo units: U1, U2 and U3) were distinguished based on grain size evolution and unconformities. Their vertical evolution is related to thrust activity in the front of the External Sierras and hence in the Gavarnie nappe (Arenas, 1993; Arenas and Pardo, 1994; Arenas et al., 2001) (Fig. 3). The units have a cyclic evolution, with a lower fining upward portion and an upper coarsening-upward portion that correspond to retrogradational and progradational stages, respectively, of the corresponding sedimentary environments (Arenas et al., 2001). The boundaries between units are major sedimentary breaks marked by a relatively abrupt changeover from coarsening- to fining- upwards trends. The sequential evolution of the alluvial deposits allows for a chronological correlation between each depositional unit and the thrust sheets uplifting the External Sierras (Arenas et al., 2001).

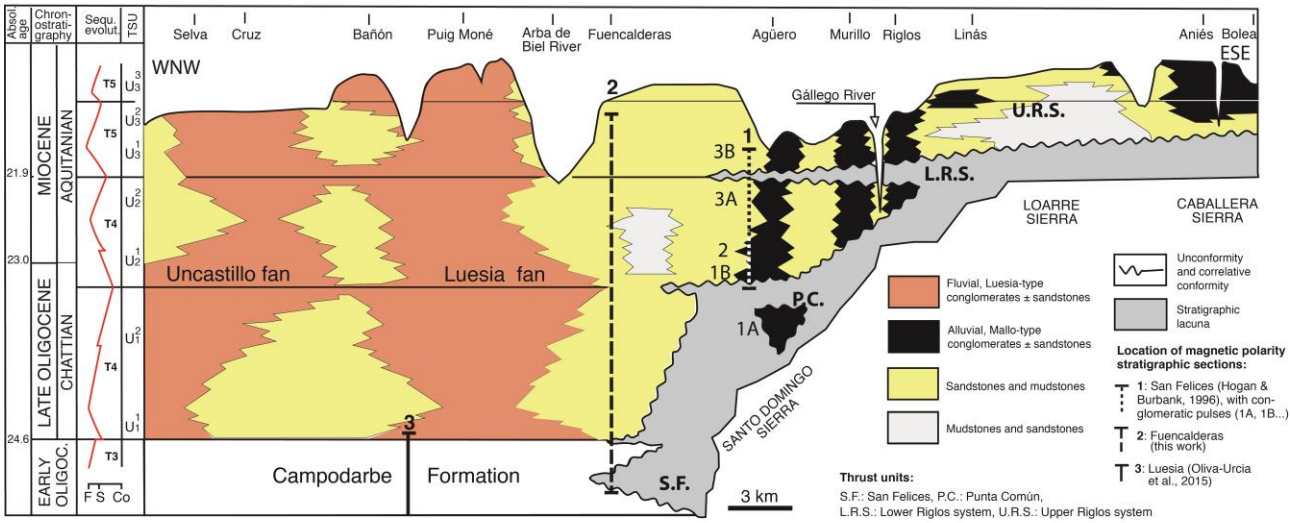

Fig. 3. Chronostratigraphic scheme showing lithofacies changes and stratigraphic relationships of the Uncastillo Fm from west to east, parallel to the basin margin. Vertical axis is not at truly time-scale but arbitrarily referred to thickness in the Luesia area. The tectonic activity in the frontal part of the External Sierras is also marked (adapted from Arenas et al., 2001).

The underlying Campodarbe Fm corresponds, in the Luesia section, to fluvial sandstones and mudstones of ESE provenance, from carbonatic and siliciclastic Mesozoic rocks (Puigdefàbregas. 1975). The new magnetostratigraphic data from the base of the section (700 m thick, san Marzal section) help constraining the marine-continental transition and to complete the magnetostratigraphy of a total of ~4 km section in the Campodarbe Fm. The previous Luesia section data (~3.3 km-thick) and discussion about ages and depositional rates can be found in Oliva-Urcia et al. (2016).

3. Methods

Two new magnetostratigraphic sections are studied in this paper, above (Fuencalderas section) and below (San Marzal section) the previous Luesia section (Oliva-Urcia et al., 2016). The lower part of the Fuencalderas section can be correlated with the previous Luesia section (ca. 3.3 km thick; Oliva-Urcia et al., 2016) by means of aerial photograph observations. The Luesia section overlaps with the San Marzal section. Altogether, the entire stratigraphic record of the basin above the Bartonian marine marls is covered in a more than 5 km thick composite section. The Fuencalderas section spans ~1000 m through the middle-distal part of the Luesia fan (Uncastillo Fm TSU 4 and 5) and about 200 m through the underlying Campodarbe Fm, part of the latter is detached over younger strata of the Campodarbe Fm in the San Felices thrust sheet. The Fuencalderas section (FU) was sampled along the dirt road leading from Fuencalderas to San Miguel de Liso Romanic hermitage (base: 42° 23' 19.7556" N. 0° 52' 23.9088" W; top: 42° 22' 6.0996" N. 0° 53' 26.0340" W) (Fig. 1 in the Supplementary material). Samples were obtained in siltstone and mudstones beds with a total of 215 magnetostratigraphic sites drilled along the ca. 1.2 km thick Fuencalderas section, with an average spacing of 7.5 m between consecutive sites. At least 2 oriented samples were obtained at each site with electrical power/cordless drills with diamond bits cooled by water. The outcrops were cleaned by digging about 50 cm deep in order to get access to fresh rocks. When these preferred muddy lithologies were absent, fine-grained sandstones were drilled instead. The drilled cores were oriented in situ with a magnetic Topochaix compass coupled to a core orienting device with clinometer. The attitudes of the bedding planes were also measured with a compass in the field, and stratigraphic thickness was measured with a Jacob's staff. GPS coordinates were also taken for every site (see Tables 1 and 2 and Figs. 1 and 2 in supplementary material).

In the new San Marzal Section, the lower part of the Campodarbe Fm (700 m), the underlying transitional Yeste-Arrés Fm (30 m) and the underlying Arguis Fm (136 m) were sampled (Fig. 2 in Supplementary material). Due to outcrop conditions, the San Marzal section is composed of two subsections, the base of first sector (Arguis Marls Fm) is at 42° 27' 53.0136" N. 0° 57' 52.7616" W and the top is at 42º 27' 53.017'' N. 0º 57' 52.783'' W. The base of the second sector is at 42º 27' 24.336'' N, 0º 58' 15.294'' W, and the top is at 42° 26' 49.4628" N. 0° 58' 20.046" W. The sampling interval is, on average, 5 m. Samples were obtained in marls, sandy marls and mudstones beds in Arguis Fm, Yeste-Arrés and Campodarbe Fms respectively. A total of 28, 7 and 142 magnetostratigraphic sites were drilled along the 836 m of the Arguis Fm, Yeste-Arrés Fm and the pretectonic Campodarbe Fm. The sampling and field methods were identical to those applied in the Fuencalderas section.

Stepwise thermal demagnetization and measurement of the NRM and rock magnetic experiments (IRM acquisition in 3 axes and subsequent IRM thermal demagnetization) were conducted at the Paleomagnetic Laboratory of Barcelona (CCiTUB – ICJTA-CSIC). At least one sample per site was thermally demagnetized using furnaces TSD-1 (Schonsted) and MMTD80 (Magnetic Measurements). Temperature increments ranged from 100 °C to 20 °C, from initial room temperature up to 680ºC. The remanence was measured in a superconducting rock magnetometer (2G Enterprises, Model 755-1.65). Characteristic components (ChRM) directions were obtained by principal component analyses (Kirschvink, 1980) after visual inspection of the demagnetization diagrams (Paldir software). additional estimations were done with the VPD software (Ramón et al., 2017), and the paleomagnetic programs Pmag1.0 written by Lisa Tauxe were used for achieving and plotting the fisherian means. For the IRM acquisition a Pulse magnetizer IM10-30 (ASC Scientific) was used and the resulting magnetization was measured using a spinner magnetometer JR6A (Agico). The results were plotted with AGICO's program Remasoft.

4. Results

The stepwise thermal demagnetization provides a maximum unblocking temperatures range from 440º to 680 ºC in most of the samples (Fig. 4), which suggests a mixture of magnetite and hematite as the main carriers of the magnetization in the continental rocks (pretectonic Campodarbe and Uncastillo Fms).

These mineralogy assemblages are also supported by the IRM acquisition curves of selected samples performed in this work (Fig. 3 in Supplementary material), IRM and 3D IRM decay curves (Lowrie. 1990) show the presence of high coercitive minerals, the IRM acquisition curves does not saturate at 1 Tesla and the 3D IRM decay curves indicate the presence of hematite (Néel temperature of 685ºC), except for FU3, with the decay of the magnetization below 600ºC (Curie temperature of magnetite). Visual inspection of the demagnetization diagrams revealed two components in most of the samples. The low temperature component was unstable below 250 º C, and it is interpreted as a present-day field viscous component. The calculated characteristic component (ChRM) isolated after removal of the viscous component, yielded both normal and reversed polarities. ChRMs were classified as good quality (class 1 and 2), when defined by more than 3 steps and/or maximum angular deviation (MAD) less than 15°. The good quality characteristic component was obtained in 84 % of the samples (Table 1). Poor quality (class 3) ChRMs were characterized by unstable, noisy trajectories in the vector end diagrams in which polarity could be hardly assessed and were discarded for further analyses.

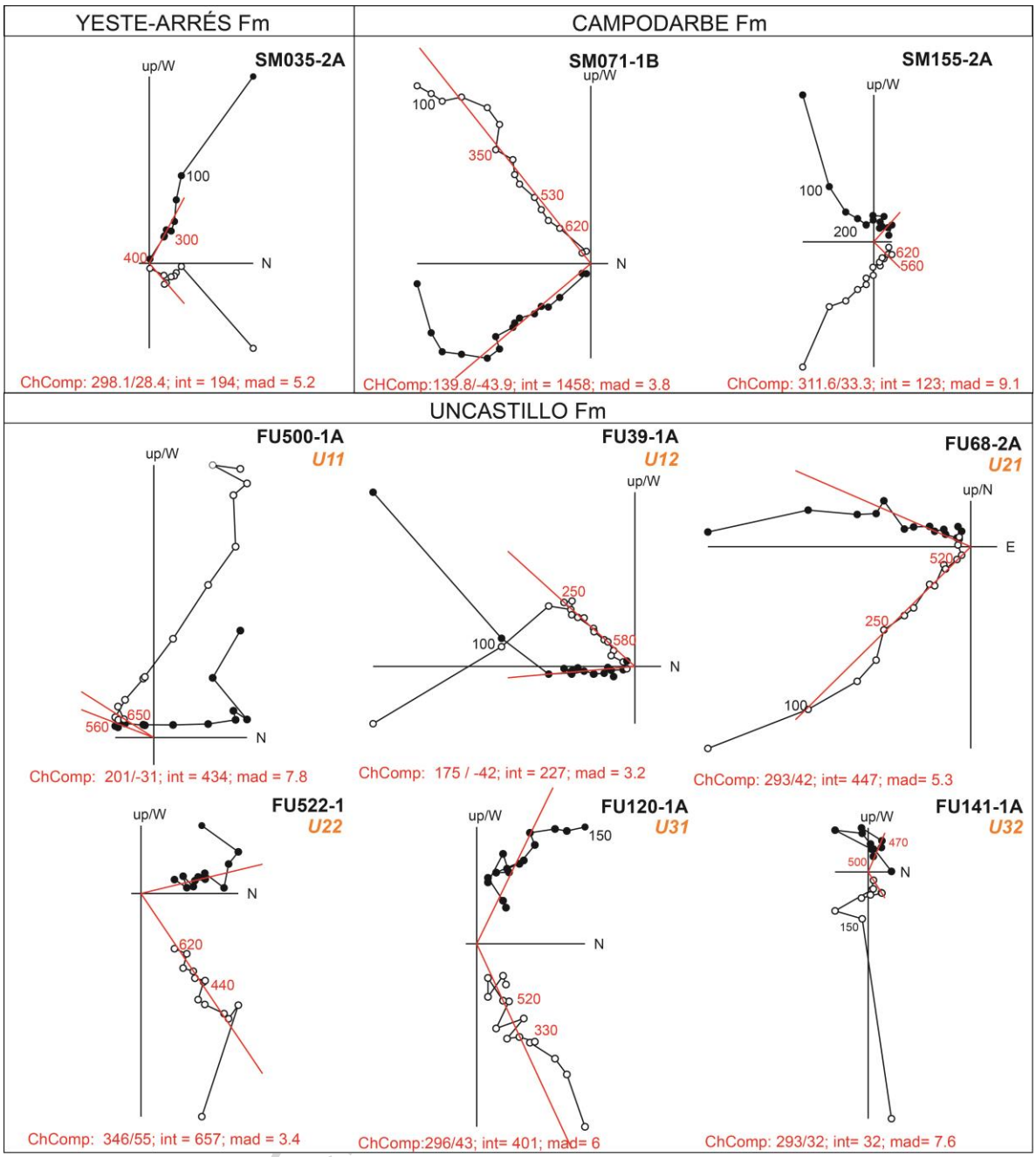

Fig. 4. Demagnetization diagrams after tectonic correction of representative samples of Yeste-Arrés Fm (transitional) and from the Cambodarbe Fm in San Marzal section (SM), and from the Uncastillo Fm in Fuencalderas section (FU). All diagrams represent stepwise thermal demagnetization, each step indicated as ºC. Red values represent the interval considered to obtain the declination and inclination of the Characteristic component (ChComp declination / inclination). NRM values (int) are expressed by 10^{-6} A/m in magnitude. MAD: maximum angular deviation.

When class 1 and 2 ChRM directions are plotted in stereographic projection after the bedding correction (Fig. 5) it can be observed a slight inclination shallowing or inconsistent declination/inclination relationships, especially in reversed directions, and that directions do not pass a reversal test. Apart from a likely inclination shallowing caused by sedimentary load, the

averaged normal and reverse components do not show a truly antipodal character. All these observations suggest that ChRM directions were not fully isolated from a recent field overprint, and therefore are partially overlapped (Rodriguez-Pintó et al., 2011). The obtained ChRMs were used to calculate the Virtual Geomagnetic Pole (VGP) latitude at sample level and plotted against stratigraphic thickness in order to build the local polarity sequence (LPS). 21 magnetozones in the Fuencalderas section, and 11 in the San Marzal section were defined by at least two consecutive sites of the same polarity; single site magnetozones were not considered reliable and they were represented as half-width bar in the LPS (Figs. 6 and 7)

SAN MARZAL SECTION

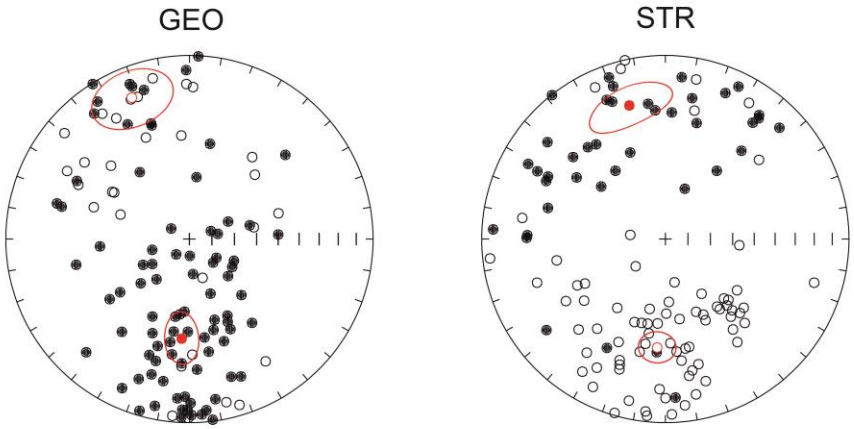

Total N = 117

Mode:	Dec,	Inc,	α95,	N,	k
1st:	184.3	44.8	8.6	80	4
2nd:	337.9	-18.0	15.1	37	3

Total N = 117

Mode:	Dec,	Inc,	α95,	N,	k
1st:	344.9	25.6	12.6	43	4
2nd:	184.3	-40.4	8.0	74	5

FUENCALDERAS SECTION

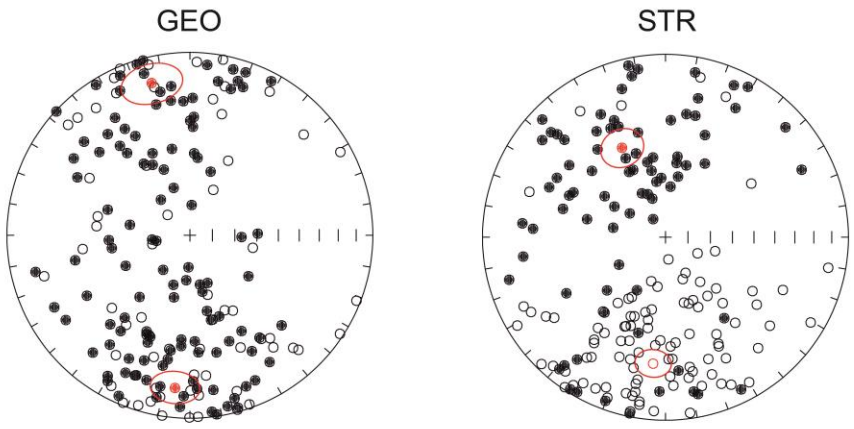

Total N = 181

Mode:	Dec,	Inc,	α95,	N,	k
1st:	345.9	15.3	10.1	70	4
2nd:	185.6	17.3	8.8	111	3

Total N = 181

Mode:	Dec,	Inc,	α95,	N,	k
1st:	334.1	44.8	9.2	71	4
2nd:	185.6	-31.2	6.8	110	5

Fig. 5. Class 1 and 2 ChRM directions of Fuencalderas and San Marzal section plotted in stereographic projection, black (white) down (up). Fisherian average of the northern and southern directions are given in geographic (GEO) and when bedding is restored to horizontal (STR). Dec: declination, Inc: inclination, α_{95} and k are statistical parameters of the distribution, N: number of samples.

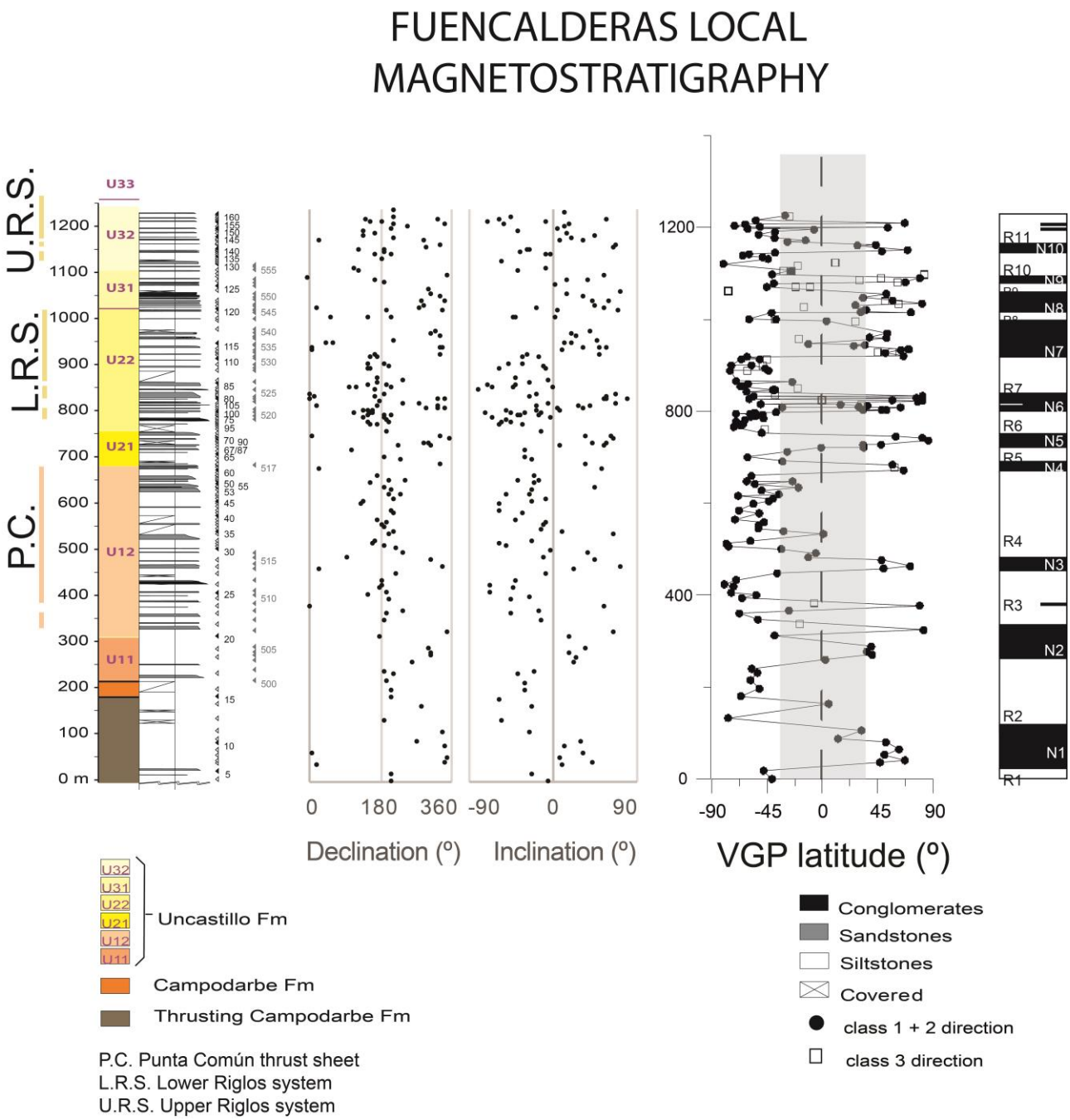

Fig. 6. Stratigraphy, Declination, Inclination, VGP latitude of the analyzed samples and local polarity sequence (LPS) described in the Fuencalderas section. Activity of thrust systems is also represented on the left.

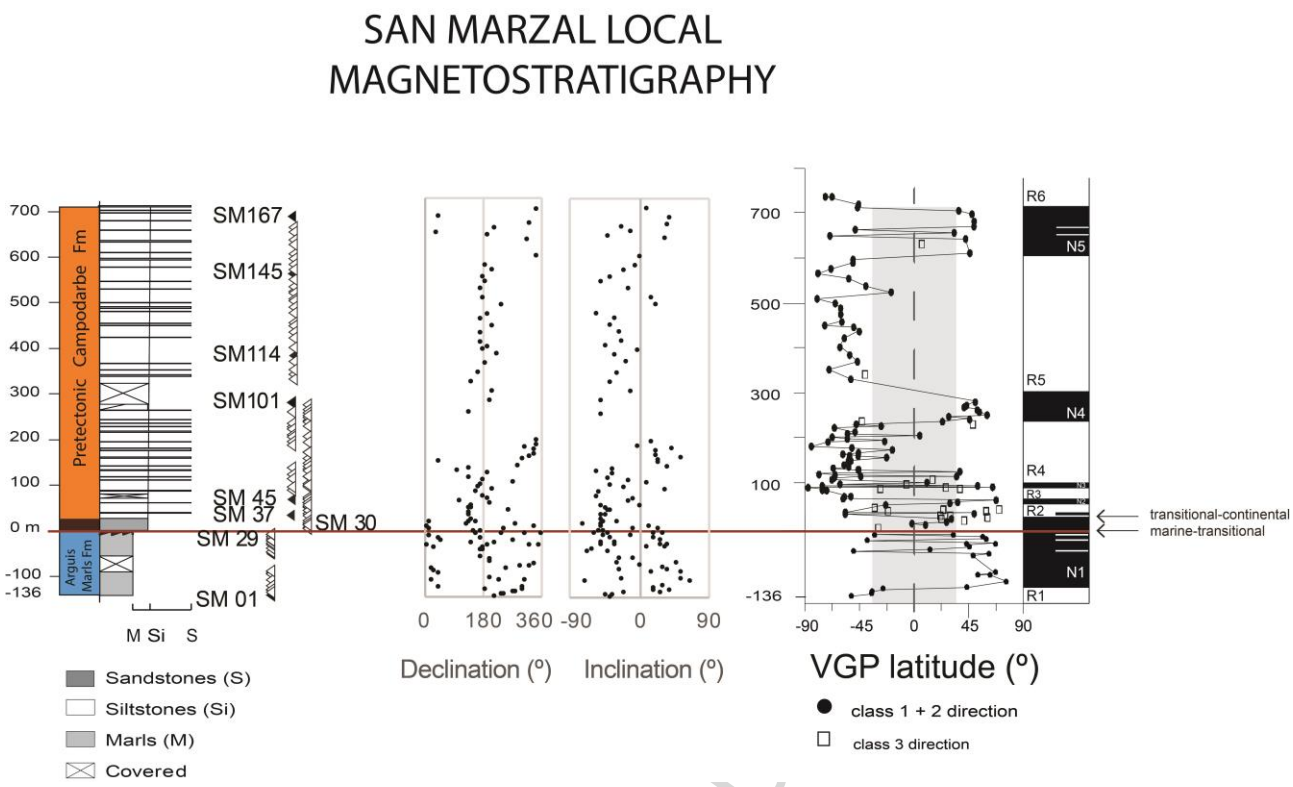

Fig. 7. Stratigraphy, Declination, Inclination, VGP latitude of the analyzed samples and local polarity sequence (LPS) described in the San Marzal section. Samples SM168 to SM177 overlap with the lower part of the Luesia section (Oliva-Urcia et al., 2016).

Correlation to the GPTS

The correlation of the local magnetozones of the Fuencalderas section (1.2 km) to the GPTS is straightforward when the chronostratigraphic constraints yielded by the nearby Luesia magnetostratigraphic section (Oliva-Urcia et al., 2016) and the new data from the bottom of the Luesia section (first 836 m, i.e., the San Marzal section) are considered (Fig. 8). The Luesia section is located only ~10 km west of the Fuencalderas section (Fig. 2a). With the new data presented in this work, it encompasses ~ 4000 m of the Campodarbe Fm, and about 50 m of the Uncastillo Fm at the top of the section. In addition, 30 m of transitional (Yeste-Arrés Fm) and 136 m of marine facies (Arguis Fm) underlying the continental deposits are also considered. This long record allowed an independent and unambiguous correlation of the Luesia-San Marzal magnetostratigraphic section to the GPTS from C16r (this work) up to C7r (Oliva-Urcia et al., 2016) and this work too. The boundary between the Campodarbe Fm and Uncastillo Fm (boundary between TSUs 3 and 4) lies within a reverse magnetozone at the top of the Luesia section, which was proposed to be correlated to C7r (Oliva-Urcia et al., 2016). Tracing this boundary by aerial photograph mapping also places it within a reverse magnetozone (R2) in the Fuencalderas magnetostratigraphic section at the bottom of the Uncastillo Fm. Thus a correlation with C7r seems the most plausible one (Figs. 7 and 8).

Magnetozones N4 to N6 of the Fuencalderas section are proposed to correlate with the characteristic normal triplet of C6C and N7-N8 are tied with the normal pair of C6B. It is worth pointing out that magnetozone N3 in the Fuencalderas section is correlated to a chryptochron within C6Cr. Although this normal event is not represented in the most recent GPTS (Ogg 2012; Ogg et al., 2016), it was compiled and referred to as C6Cr-1 in the CK95 GPTS (Cande and Kent, 1995). Moreover, it has been also reported in other magnetostratigraphic sections in continental records of the Ebro Basin (Barberà et al., 1994; Valero et al., 2014). From this correlation, the age of the Uncastillo Fm in the Fuencalderas section is Chattian to Aquitanian, and ranges from 24.55 Ma (boundary between units TSU3 and TSU4, being TSU4 the local unit U1-) to 21.2 Ma (which is the top of the studied section at Fuencalderas, in the middle part of local unit U32). The boundary between local units U2 and U3 (i.e., the boundary TSU4 / TSU5) occurs at 21.95 Ma. (Fig. 7, 8). The San Marzal section (underneath the Luesia section in Oliva-Urcia et al., 2016) comprises the C16 to C13, where the local magnetozone N1 (Arguis Marls Fm) corresponds to the long C16n. The N4 and N5 local magnetozones of the San Marzal section from the pretectonic Campodarbe Fm clearly correlate to the normal C15 and C13 respectively. Therefore, the definitive marine to continental transition of the pretectonic Campodarbe Fm occurs at ~36 Ma (35.8 Ma) (Fig. 8) in agreement with Costa et al. (2010).

The correlation of 5 km thick section to the GPTS enables timing the thrust systems active during the deposition of the local units U1 to U3. Activity of the Punta Común thrust sheet ranges from 24.2 Ma to 23.25 Ma. Lower Riglos thrust system activity also lasted ~1 My, from 22.9 to 21.9 Ma and activity in the Upper Riglos thrust system initiated soon after 21.6 Ma (Figs. 6 and 9).

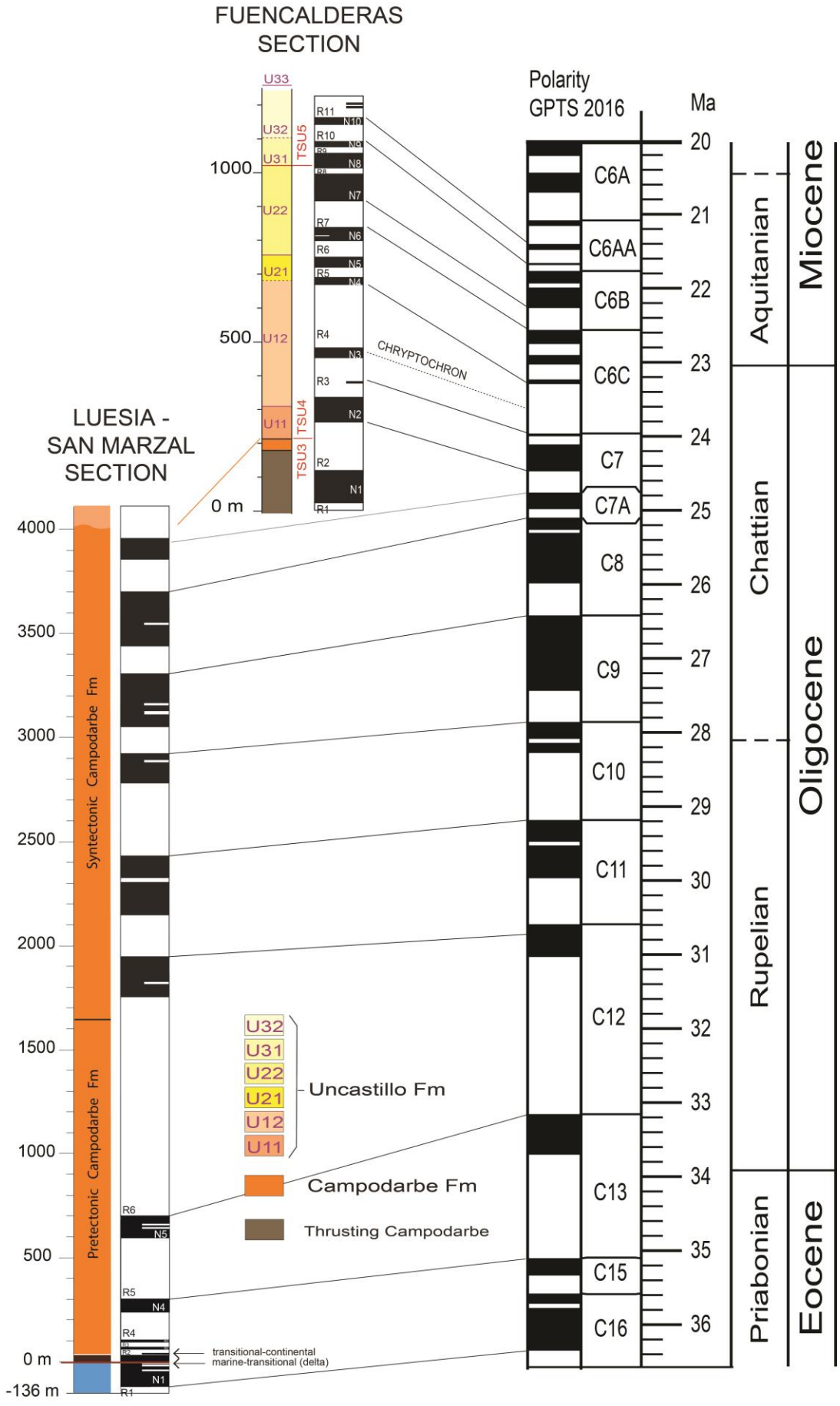
FUENCALDERAS
SECTION
LUESIA -
SAN MARZAL
SECTION
Polarity
GPTS 2016
Ma
U33
U32
U31
U22
U21
U12
U11
TSU5
TSU4
TSU3
1000
500
0 m
R11
N10
R10
N9
N8
N7
R7
N6
R6
N5
R5
N4
R4
N3
R3
N2
R2
N1
R1
CHRYPTOCHRON
4000
3500
3000
2500
2000
1500
1000
500
0 m
-136 m
Syntectonic Campodarbe Fm
Pretectonic Campodarbe Fm
U32
U31
U22
U21
U12
U11
Uncastillo Fm
Campodarbe Fm
Thrusting Campodarbe
transitional-continental
marine-transitional (delta)
C6A
C6AA
C6B
C6C
C7
C7A
C8
C9
C10
C11
C12
C13
C15
C16
20
21
22
23
24
25
26
27
28
29
30
31
32
33
34
35
36
Aquitanian
Chattian
Rupelian
Priabonian
Miocene
Oligocene
Eocene

Fig. 8. Correlation of the Fuencalderas section to the GPTS2016 (GPTS done with TSCreator visualization of enhanced Geologic Time Scale 2016 database, version 7.3. https://engineering.purdue.edu/Stratigraphy/tscreator). The Luesia section (Oliva-Urcia et al., 2016) and the new results of the first 836 m of the bottom of the Luesia section (San Marzal Section) are also represented.

5. Discussion

The syntectonic infill of foreland basins informs about the external factors that influence deposition, i.e., stages of the deformation in the orogeny and the climate in the region. In particular, at the margins of the basins, the architectural geometry of the strata can be genetically linked to specific structures (thrust sheets and folds); for example, when there is a coincidence between alluvial fan progradation into the basin and structural shortening (causing a coarsening upward in grain size evolution). Then, climatic influence is ruled out, and a tectonic coupling is deduced (Heermance et al., 2007). In this scenario, the latest succession of deposits in the northern Ebro Basin (Uncastillo Fm) and its tilting has been related to distinct tectonic movements (thrusts) in the External Sierras, the southwestern frontal thrust of the Pyrenees (Arenas et al., 2001). Part of the underlying Campodarbe Fm and its tilting is also directly related to the tectonic activity in the southern deformation front with the San Felices thrust sheet and with the younger development of the Santo Domingo anticline as deduced in Puigdefàbregas (1975), Millán et al. (2000) and Pueyo et al. (2002). Dating the continental deposits at the margins of the Ebro foreland basin will then, in turn, help to constrain the tectonic events at the front of the orogen in combination with previous kinematic interpretations (Labaume et al., 2016). The timing of the tectonic activity in the orogen will help to delimit the architectural facies distribution in an endorheic foreland basin when compared with the sedimentary infill at the center, which shows the climate forcing in the lacustrine sedimentary sequences (Arenas and Pardo, 1999; Valero et al., 2014).

5.1.Accumulation rates

It has been considered that abrupt changes in sedimentation rates are either related to tectonic activity, changes in the accommodation space and/or in the flux of sediments due to climate influence (Riba, 1980; Molnar, 2001; Peizhen et al., 2001). Models constructed to characterize the sedimentary changes and geometry of sedimentary units found in the sedimentary record of foreland basins are related to either changes in precipitation or fault slip rates (Armitage et al., 2011). The response of the sediments to a changing tectonic regime is more diverse and punctuated

than to a change in precipitation in the catchment area (different climate), that is, an increase in the uplift rate results in larger grain size deposition in proximal sites, followed by finer grain size at distal locations. However, an increase in precipitation in the catchment area results in deposition of a laterally extensive sheet of coarse gravel (Armitage et al., 2011). In alluvial fans, precipitation changes do not affect accumulation rates as much as tectonic activity does. However, sediment flux along the alluvial fan varies rapidly with precipitation changes and more slowly with tectonic activity (0.5 – 2 Myr) (Densmore et al., 2007). Nonetheless, the rapid changes due to precipitation are more difficult to detect in proximal alluvial facies, as discussed by Pérez-Rivarés et al. (2018). Accumulation rates are deduced with the new data for the northern sector of the Ebro Basin. Then, a comparison with other previously published data from the central part of the Basin and its southwestern basin margin are considered. The variation of the accumulation rate through time is also plotted to visualize the changes in tendency of accumulation rate (Fig. 9).

The correlation of the local magnetostratigraphy with the GPTS (Fig. 8) provides ages for every local TSU sampled in the Fuencalderas section (Uncastillo Fm), and therefore accumulation rates can be calculated for the local and youngest units in the northern margin of the Ebro basin (Fig. 9.b). The highest sedimentation rate occurs in unit U12 (U12 spans from 24.2 to 23.25 Ma; 39.3 cm/kyr), when Punta Común thrust sheet (P.C. in Fig. 9.b) was active, and the lowest one occurs in unit U21 (U21 spans from 23.25 to 22.9 Ma; 22.4 cm/kyr), a time of tectonic quiescence between the Punta Común thrust and the Lower Riglos system activities (L.R.S. in Fig. 9.b). The beginning of local unit U31 at ~22 Ma (TSU5) is coeval with an increase in the accumulation rate (from 25.9 to 32.1 cm/kyr).

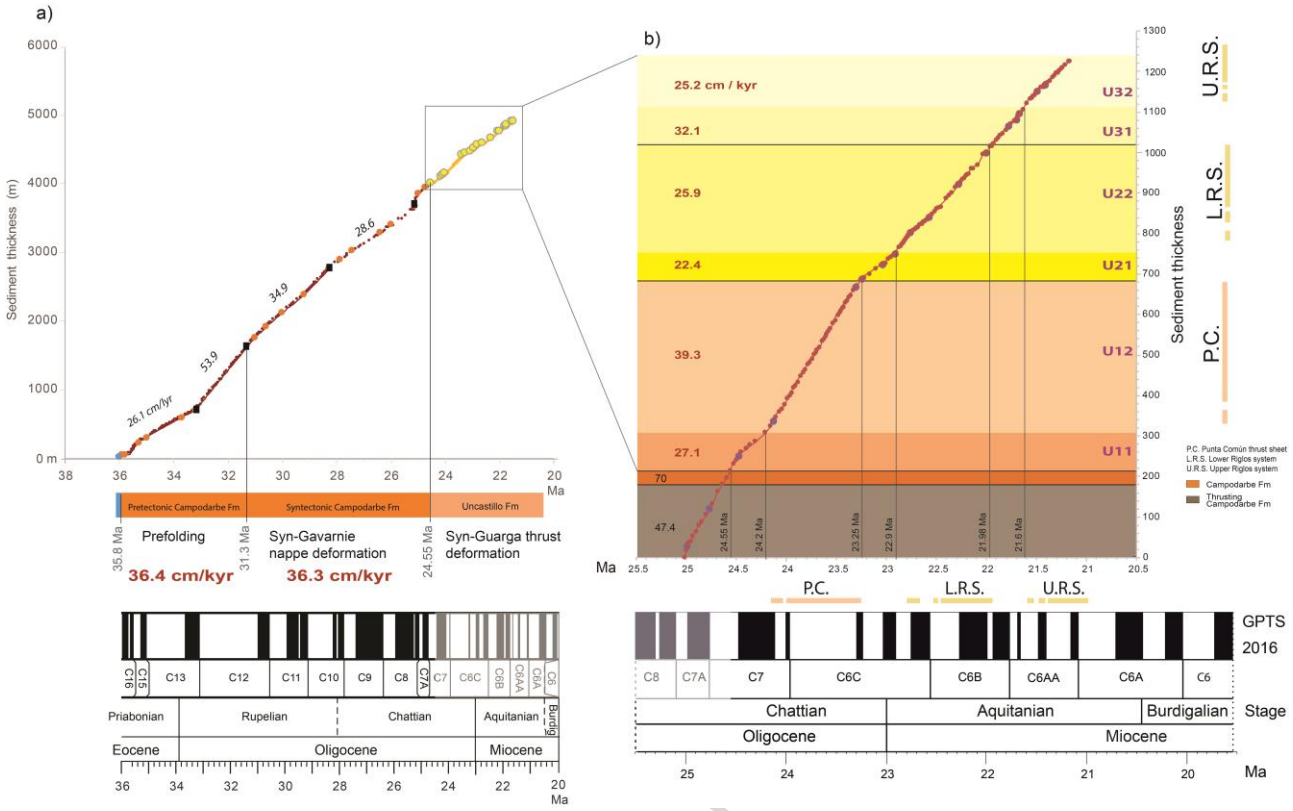

Fig. 9.a) Accumulation rates for San Marzal-Luesia (Campodarbe Fm) and Fuencalderas (Uncastillo Fm) sections and the activity of thrust sheets in the Uncastillo Fm during deposition. Black squares are the limits to calculate the accumulation rate written next to the graph. b) Accumulation rates of the Uncastillo Fm for every local tectosedimentary unit. The activity of the thrust sheets affecting the sedimentation in the Uncastillo Fm is marked in age and sedimentary thickness. Large dots are actual data, and small dots are linearly interpolated data (Analyseries 2.0.8 software).

Accumulation rate values in the Uncastillo Fm vary from ca. 39 to 22 cm/kyr and are comparable to the underlying Campodarbe Fm accumulation rates calculated in Oliva-Urcia et al. (2016), which vary from 35 to 27 cm/kyr. When considering the accumulation rates for both the pretectonic and syntectonic Campodarbe Fm, the values are similar: 36.4 and 36.3 cm/kyr, respectively (Fig. 9.a). When taking into account the variations in the slope of the graph in Fig. 9a, accumulation rates increase from ca. 26 to ca. 54 cm/kyr, at 33.1 Ma and decrease to ca. 35 cm/kyr at 31.3 Ma and decrease again to 28.6 cm/kyr at ca. 28 Ma. In general, these values of accumulation rates are of the same order of magnitude than the ones found in the final filling stages of other foreland basins at their margin with the orogen, e.g., ~50 cm/kyr in the Southern proximal part of the North Alpine Foreland Basin (Swiss OSM) (Schlunegger et al., 1997; Willet and Schlunegger, 2010); 28 to 43 cm/kyr in the Xiyu Fm. North and South of the Tianshan Mountains, in the Junggar foreland Basin (Li et al., 2011) and in the NW of the Tarim basin (Heermance et al., 2007) respectively. However,

closer to the Himalaya Orogen, in the SW Tarim Basin, the values of sedimentation rates for the Xiyu Fm twofold, rising to 111 cm/kyr (Zheng et al., 2000; 2006). In the syntectonic conglomerates incorporated to the South Pyrenean Central Unit, sedimentation rates in the Late Lutetian (~42 Ma) reach 30 cm/kyr, coupled with exhumation rates of 0.3 km/Myr (Beamud et al., 2011).

Nonetheless, our results significantly differ from those found for younger TSUs in the central part (related to the Luna and Huesca fluvial systems, from the Pyrenees) and southwestern part of the Ebro basin (related to the Los Fayos alluvial system, from the Iberian Ranges), with a sudden decrease of accumulation rates in TSU5, 6 and 7 respect to units TSU3 and 4 (Fig. 10d). The distal alluvial and carbonate lacustrine deposits related to the Luna fluvial system (in the area of Montes de Castejón (MC) –Esteban, Sora sections–; Figs. 1. 10) yielded 7.2 cm/kyr for TSU6 (TSU6 from 16 Ma to 14.6 Ma), according to data provided by Pérez-Rivarés et al., (2004) and Pérez-Rivarés et al. (2018). To the east, the distal alluvial and carbonate and sulphate lacustrine deposits in the Sierra de Alcubierre (SA) –Lanaja, Albalatillo, San Caprasio sections– (Figs. 1, 10) provided sedimentation rates of 9 and 6.8 for TSU5 (TSU5 from 21.3 to 16.3 Ma) and TSU6 (TSU6 from 16.3 Ma to 14.4 Ma) respectively (Pérez-Rivarés et al., (2004) and Pérez-Rivarés (2018). The sedimentary evolution in this part of the basin was linked to the Huesca fluvial system, sourced from the South-Pyrenean Central Unit (Fig. 1b). Averaged out accumulation rates deduced in the central part of the basin to the west, in Bardenas Reales (BR –Composed Tudela section– deduced by Larrasoaña et al., 2006) reached 14.1 cm/kyr for TSU5 (ca. 20 Ma to ca. 16 Ma), slightly higher than those of the Sierra de Alcubierre and Montes de Castejón values (Pérez-Rivarés et al., 2002; 2004; 2018 and references therein). The complete record of TSU7 (from 14.2 Ma to 12 Ma) is at the Iberian margin of the Ebro basin (south-west central part of the basin), at the Los Fayos, near Tarazona (TA –Umbría Alta, Lugar-Melero sections; Pérez-Rivarés et al., 2018 and references therein), were the proximal and medial alluvial facies deposited at a rate of 9.8 cm/kyr (Pérez-Rivarés, 2016).

In contrast, average accumulation rate for TSU3 (from 24.55 Ma to younger than 21 Ma) was 35.9 cm/kyr whereas TSU4 (from ca. 36 Ma to 24.55 Ma) showed an averaged accumulation rate of 37 cm/kyr in the Luesia (including San Marzal section) and Fuencalderas section (FU-LU), this work.

The low rates for TSU7 in the Iberian margin (Los Fayos) can be due to the fact that the Iberian ranges became a mainly passive margin compared to the Pyrenees since the deposition of TSU5 onwards. e.g., with onlap of the successive units (Pérez et al., 1988). However, along the same mountain belt, different accumulation rates can occur if drainage areas are on different catchments, as is the case of the Luna and Huesca fluvial system, which was suggested by Pérez-Rivarés et al. (2018) to explain the small diachroneity of the boundaries between units in several areas of the

basin. The variable accumulation rates between the several areas can be attributed to the different characteristics of the drainage / catchment areas in relation to the tectonic activity and topography.

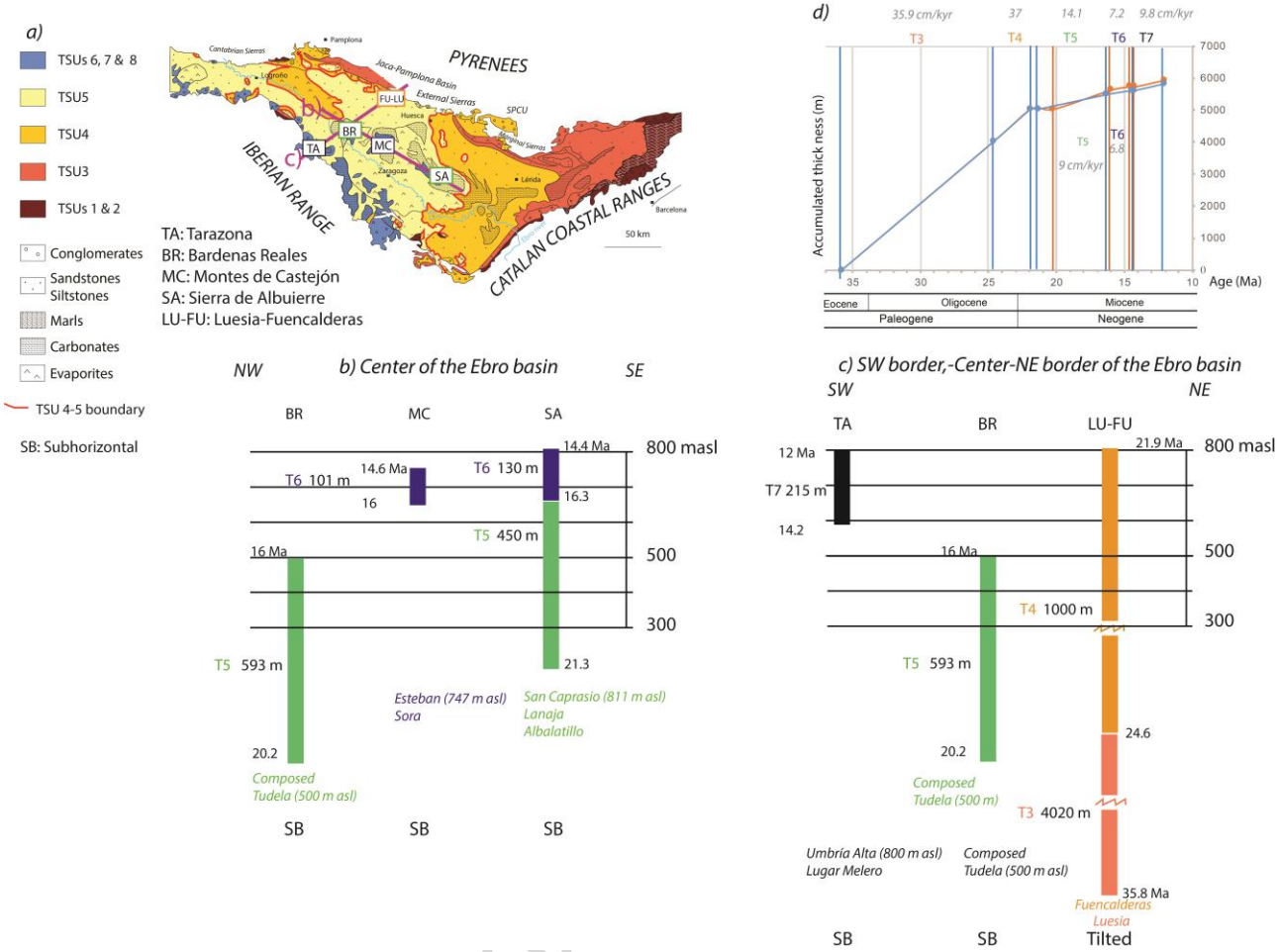

Fig. 10. a) Location of sections (Pérez-Rivarés et al., 2018 and references therein) used to calculate the accumulation rates in the Ebro basin (d), b) and c) represent the different TSU along two sections considering, approximately, the present day the altitude (black horizontal lines in masl) and thickness of studied sections (colored bars) in meters (m). In addition, dates (in Ma) of bottom and top of sections are added to the colored bars. In b) the section is located through the center of the basin with a NW-SE strike and in c) the section has a NE-SW strike. d) Averaged accumulation rates, in blue the sections of FU-LU, BR, MC, and TA. In orange, the sections of LU-FU, SA and TA. Information about tilting of bedding is also added: SB: subhorizontal. Tilted: beds are deformed.

The trend we observed concerning the deposition of TSUs (Fig. 10.b and c) is that the the first record of the deposition of TSU5 is younger in the central - southeastern sector of the basin (SA sector), whereas the the first record of the deposition of TUS6 is similar for the central axis of the basin (MC and SA sectors), without considering subsurficial data. In general, the flexural behavior of the lithosphere will affect the variable accumulation rates of sediments due to the related

accommodation space. Flexure, together with the influence of topographic load, will produce larger subsidence in the northern margin of the Ebro basin (Brunet, 1986; Lanaja, 1987; Millán-Garrido et al., 1995b; Gaspar-Escribano et al., 2001). The infill of the foreland basin during Lower-Middle Eocene occured through a strongly subsident turbiditic trough, which were located in the Southern Pyrenean foreland, due to the beginning of the subduction of the Iberian crust underneath the European crust and the surficial load (equivalent to tectonic/topographic load) (stage III in Puigdefàbregas et al., 1992). The infill during Upper Eocene-Oligocene was produced, mainly, with continental deposits and a decrease in the subsidence (stage IV in Puigdefàbregas et al., 1992), although the total continental sediment thickness reaches ca. 6 km in thickness (Fig. 10.d).

The crustal root of the Pyrenees imaged by geophysical data accounst for the lithospheric flexure (Kamer and Watts, 1983; Casas et al., 1997; Chevrot et al., 2014a). The load exerted by the subducted thin continental Iberian lithosphere up to ~70 km depth is imaged by teleseisimic wave data in two transects of the Pyrenees, revealing the importance of the rift development orthogonally to the Pyrenees trend during the Mesozoic (Chevrot et al., 2014a; 2014b).

The general trend from Late Eocene till Middle Miocene of the lacustrine systems that developed in the center of the Ebro foreland basin (Fig. 1 in Valero et al., 2014 and references therein), would also be influenced by i) the flexure of the lithosphere through the opening of the Valencia trough (from Late Oligocene to Neogene) as represented in Fig. 3 of Gaspar-Escribano et al. (2001) and ii) climate (Arenas and Pardo, 1999, 2000; Valero et al., 2014).

5.2.Dating the tectonic activity

5.2.1. Younger ages for the latest tectonic activity (Uncastillo Fm)

Dating the Uncastillo Fm by magnetostratigraphy allows dating the deformation affecting these sediments thanks to previous studies that defined tectosedimentary units (TSU) in the Luna fan deposits. These TSU are related to cover thrust sheets affecting the frontal part of the Pyrenean orogen in the External Sierras (Arenas et al., 2001).

The Uncastillo Fm was previously sampled for magnetostratigraphic studies east of the Fuencalderas section, in San Felices, Agüero and Ayerbe sections (Hogan and Burbank, 1996) (left side of Fig. 11). These previous sections were of ~ 500 m thick in San Felices and Ayerbe sections and ~200 m thick in Agüero section. The new magnetostratigraphic data obtained from the Fuencalderas section (~1000 m) provide an age for the Uncastillo Fm of 24.6 Ma (beginning of unit TSU4, at the base of local unit U1) to 21.6 Ma (the boundary of local units U31-U32), and new dates for the tectonic activity in the External Sierras considering Arenas et al. (2001). Younger ages of ~ 5.4. ~1.5 and ~1 Myr compared to the ones deduced by Hogan and Burbank (1996), are found

for the beginning of the deformation connected to the Punta Común thrust sheet (from bottom of C10 to bottom of C6C, that is from 29.4 Ma to 24 Ma), theLower Riglos thrust sheet system (from C6C to C6B, from 24 to 22.5 Ma) and the Upper Riglos thrust system (from C6B to C6A, from 22.5 to 21.4 Ma) respectively (Fig. 11).

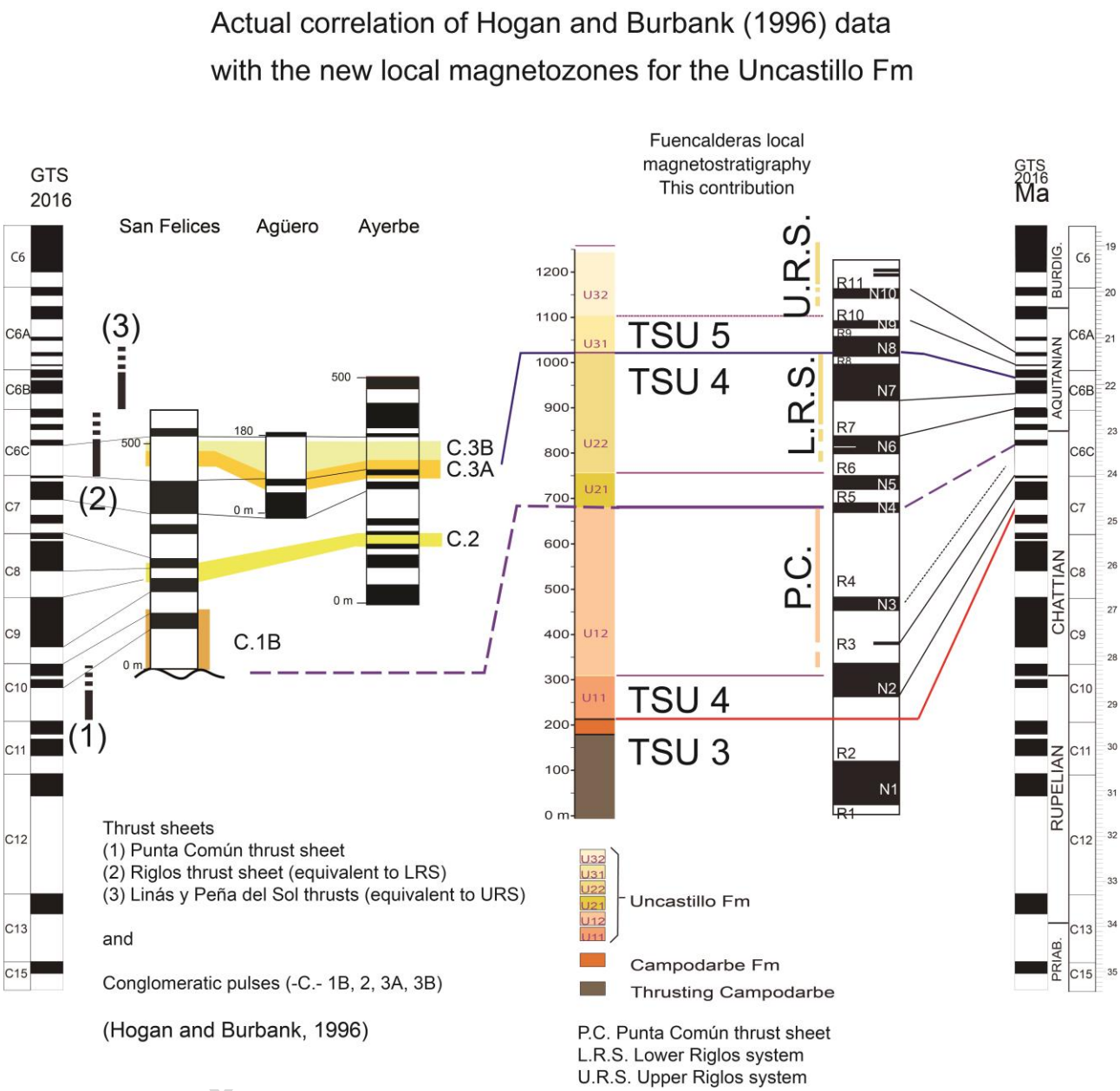

Fig. 11. Comparison of ages for the beginning of the activity of the thrusts affecting the Uncastillo Fm. Hogan and Burbank (1996) on the left, this work on the right. All ages are compared to GPTS 2016.

5.2.2. Timing of deformation, changes in accumulation rates; Ebro basin -Pyrenean orogen

The Pyrenean Range is an asymmetric double vergent collisional mountain chain formed from late Cretaceous to early Miocene (Roure et al., 1989; Choukroune et al., 1989; Muñoz, 1992; Vergés et

al., 2002) Fig. 12. Topographic load in the Pyrenees doubled from Paleocene to Oligocene and remained almost stable through Oligocene and Neogene (Curry et al., 2019). According to paleoelevation records from stable isotope data from Eocene marine oyster shells, an elevation gain of 2000 m is deduced to have occurred from 49 to 41 Ma ago, therefore, a topography similar to the present day Pyrenees is present since the Eocene (Huyghe et al., 2012). Recent 3D flexural modeling by also suggests that modern topography was achieved by the end of the Eocene (Curry et al., 2019). The deposition of the Campodarbe Fm was influenced by this already formed topography, generating a WNW directed flux of sediments (Puigdefàbregas, 1975). Similar results in paleotopography of 1-2 km of paleoelevation on the water divide at the leading edge of the non-subducted European plate, are deduced from the 2D flexural modelling based on 2 time slices of crustal-scale cross-sections (Millán et al., 1995b). Discussion about the evolution of relief through highly elevated peneplains in the eastern part of the Pyrenees reveal that this subject is still a matter of interest but unresolved (Babault et al., 2005; Gunnell and Calvet, 2006). Elevation in the External Sierras is deduced to be mainly associated with the final tightening of the Santo Domingo anticline, coeval with the Uncastillo Fm deposition (Millán-Garrido et al., 2000). The general structure in the western part of the Pyrenees comprises south vergent basement thrust units in the Axial Zone that connect with Mesozoic and Paleogene-Neogene thrust units to the south, which represent the South Pyrenean Zone (SPZ). The SPZ overrides the Ebro foreland basin (Labaume et al., 2016 and references therein; Labaume and Teixell, 2018; Muñoz et al., 2018). Chronology of the deformation is deduced from growth strata and angular unconformities of syntectonic deposits, field observations, geometrical features of basement units and displacement transfer considerations (Riba, 1976; Ford et al., 1997; Arenas et al., 2001). The combination of former data with previous apatite fission track thermochronology allows cautiously, deducing the exhumation history of the Pyrenees in the west central part at a distance of ~40 km east of the new magnetostratigraphic data, as follows: 1) From Lutetian to Bartonian (ending at ~38 Ma) the propagation of the Eaux-Chaudes/Monte Perdido thrusting in the Jaca Basin occurs. Later, the Gavarnie basement unit develops while the growth of the N-S detachment folds of the Sierras Exteriores continues until the Priabonian. 2) Priabonian to early Rupelian corresponds to the Gavarnie basement thrusting, transferred into the Oturia and Yebra de Basa cover thrusts (until ca. the end of the C12 reversal, ~31 Ma). At the same time, deposition of the upper part of the Hecho Group, the Arguis-Pamplona marls, the Belsué-Atarés deltaic sandstones, and the lower part of the Campodarbe fluvial-alluvial deposits occurs. 3) Rupelian-early Chattian with the displacement of the Broto basement thrust sheet (equivalent to the Bielsa basement thrust sheet –Martínez-Peña and Casas-Sainz, 2003- to the east) and the deposition of the upper part of the Campodarbe Fm. 4) Chattian-early Miocene (ending at ~20 Ma) corresponds to the activity of the Fiscal and Guarga basement thrusts, which are

responsible for the displacement on the frontal ramp in the Sierras Exteriores (Labaume et al., 2016 and references therein) and the deformation recorded in the continental deposits of Campodarbe and Uncastillo Fms (Fig. 11 and graphical summary).

The onset of the syn-Gavarnie nappe deformation (Broto and Fiscal basement thrusts) recorded by the continental deposits (Campodarbe Fm) occurred with the San Felices thrust sheet, during early to middle Rupelian (Oligocene), starting at 31.3 Ma in the Luesia section (Oliva-Urcia et al., 2016). Later, the syn-Guarga thrust deformation affected the tightening of the Santo Domingo anticline in the External Sierras from 24.55 Ma to 21.2 Ma in the Fuencalderas section (Uncastillo Fm, this work and Oliva-Urcia et al., 2016) whereas the activity of the Punta Común and Riglos thrust systems occurred from 24 to 23.5 Ma in the Fuencalderas section (Chattian, Oligocene) and that of the Riglos system intermitently from 22.7 to 21.2 Ma (Aquitanian, Miocene) respectively (as seen before).

Derivative of the accumulation rate respect to time stands for the acceleration/deceleration of sediment accumulation rate (Fig. 12.c). The comparison of variations in the derivative of the accumulation rate from the LU_FU sections at the boundary basin-orogen with the tectonic activity in an area ~40 km more to the east (Fig. 12.d, data from Labaume et al., 2016) allows to suggest correlations between these two variables and tectosedimentary relations can be deduce.

For example, there is an acceleration of the accumulation rate at the continentalization of the foreland basin (~36 Ma. Costa et al., 2010), that is, in the studied area, the LU-FU sections, and at the beginning of the sedimentation of the Campodarbe Fm, when the Oturia thrust sheet was already active and the Yebra de Basa cover thrust sheet started its movement (Labaume et al., 2016). There is also a sharp increase in the trend of the derivative of the accumulation rate respect to time at ~33 Ma, i.e., at the time of the increase in the accumulation rate from ca. 26 to ca. 54 cm/kyr (Fig. 9), which seems coeval with the beginning of the tectonic activity of the Broto basement thrust. In contrast, at ~31.3 Ma (Rupelian), by the end of the Yebra de Basa cover thrust sheet, and at the beginning of the activity of the San Felices cover thrust sheet (Oliva-Urcia et al., 2016 based on Puigdefàbregas 1975), a subtle deceleration of the accumulation rate with time occurs, coinciding with a decrease of the accumulation rate (from ca. 54 to ca. 35 cm/kyr, Fig. 9a), although there is no change in the sedimentary facies according to Puigdefèbregas (1975). A decline in the accumulation rates together with a progradation of proximal continental facies (increase of the proportion conglomerates/lutites of an alluvial fan) tend to suggest a reduction in the accommodation space (Jones et al., 2004; Beamud et al., 2011). A similar situation occurs at younger ages, ca. 28 Ma, when a deceleration of the accumulation rate with time and in the accumulation rate from ca. 54 to 28.6 cm/kyr can be linked to beginning of the Fiscal / Guarga

basement thrust sheets activity. Finally, general variations in the accumulation rate with time of the Uncastillo Fm are related to the latest activity of the External Sierras.

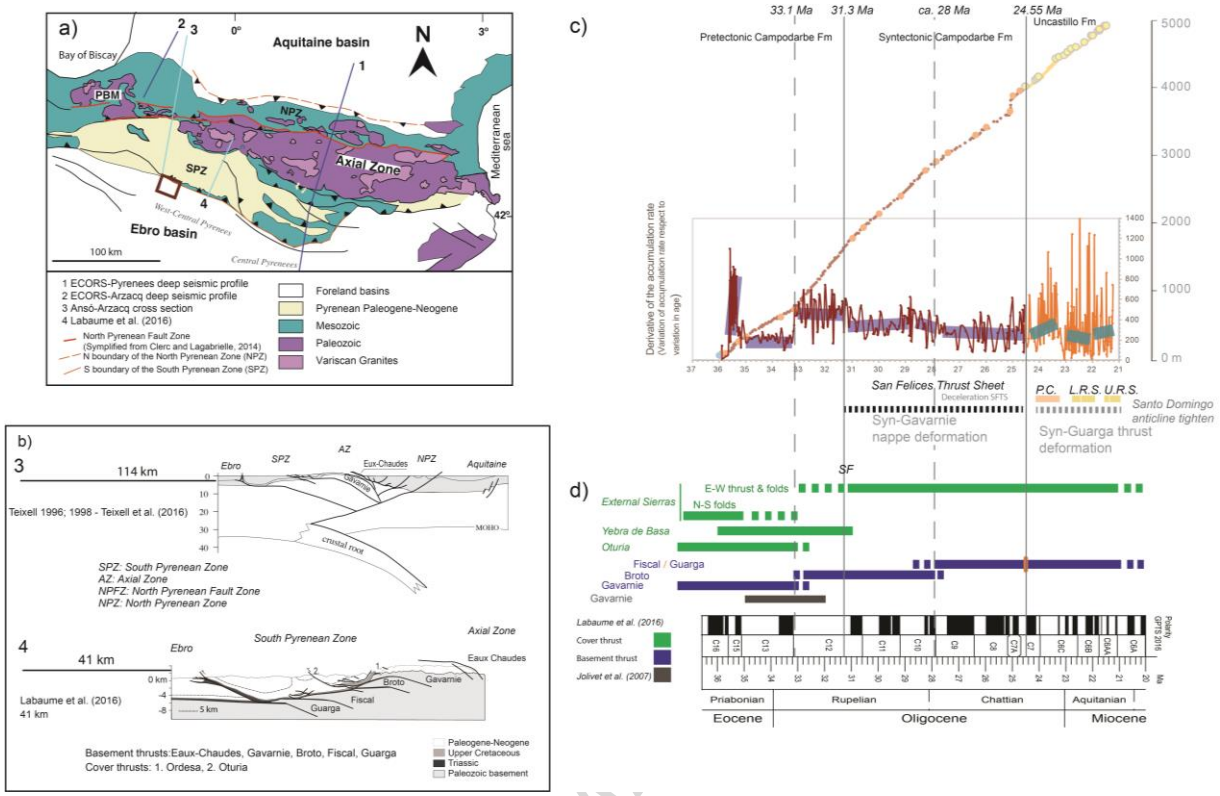

Fig. 12. a) Geological map of the Pyrenees with the location of the two geological cross-sections presented in b). The red quadrangle marks the studied area. Shortening is represented on the left of the cross-sections. c) Derivative of the accumulation rate with time respect to time with accumulation rates in the background (from Fig. 9). The derivative of the accumulation rate is $\delta y/\delta x$, where δy is the difference in thickness between two neighboring sites and δx the corresponding difference in age of the same sites. d) Chronology of the different thrust sheets from Labaume et al., 2016 and references therein in green, blue and grey bars, adapted to the data of this work. Bars in black and yellow, from this work and Oliva-Urcia et al. (2016).

5.2.3. Evolution of deformation in the SW Pyrenees: variation of bedding tilt

The variation of the tilt of the bedding planes (Fig. 13) shows very graphically the tectonic activity in the frontal part of the Pyrenees. These changes of tilt through time become apparent in the syntectonic unit of the Campodarbe Fm. The Campodarbe Fm presents quite constant vertical/slightly overturned strata in the pretectonic Campodarbe unit, whereas the bedding tilt in the syntectonic Campodarbe unit gradually decreases in the San Marzal-Luesia sections (Fig. 13b). The latest tectonic activity results in the progressive tilting of the beds of the Luesia fluvial fan up to the present day subhorizontal configuration (cross section in Fig. 13a). The variation rate of the

bedding plane tilt with time in the Uncastillo Fm (Fig. 13c) reflects the latest tectonic activity in the frontal part of the Pyrenees, with the progressive unconformity showing changes from 85º to 7º S (Figs. 13 a and b).

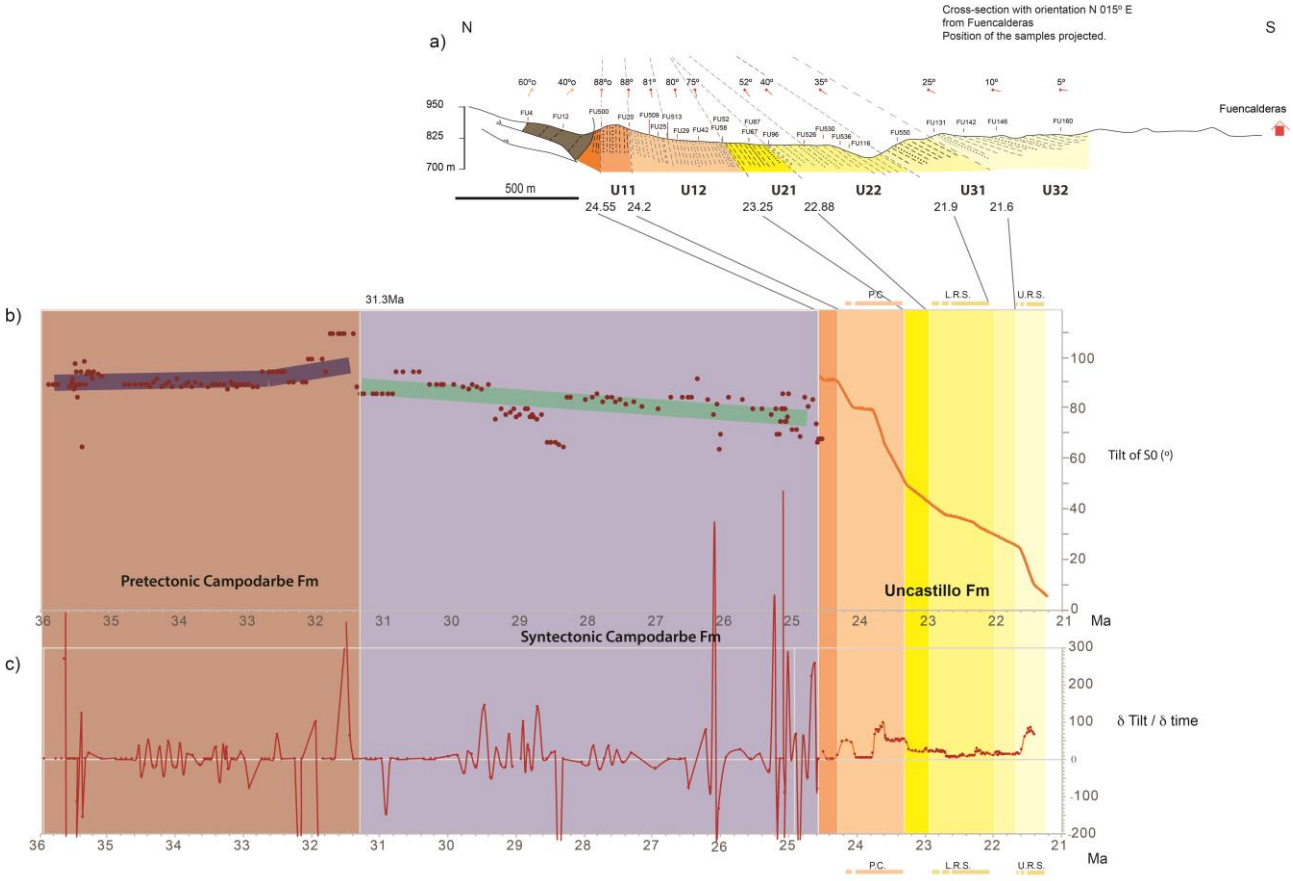

Fig. 13. a) Cross section with bedding tilt variation from N to S in the Fuencalderas section (see Fig 2a for location). b) Variation of bedding tilt respect to age from Campodarbe and Uncastillo formations. Colored lines are a visual approximation. c) Rate of tilt respect to time plotted against time (derivative of the tilt variation, calculated by δy/δx, where δy is the difference in bedding tilt between two neighboring sites and δx the corresponding difference in age of the same sites). Linear interpolation in the Uncastillo Fm has been calculated with Analyseries 2.0.8 software.

Considering the variation rate of the bedding tilt through time in the Uncastillo Fm (Fig. 13c), it is possible to see that "acceleration" of the tilt variation occurs during two episodes during the activity of the Punta Común thrust activity (from ca. 24 to 23.2 Ma, end of Chattian, Oligocene), with a tilt variation of bedding of ca. 40º (Fig. 13b). This period also shows the highest accumulation rate of the Uncastillo local units (U12). A progressive decrease of the tilt variation with time during the deposition of U21 is seen (the tilt variation of bedding is less than 10º during the time of local unit U21 is deposition). A much smaller variation occurs at the end of the LRS (Lower Riglos system) but with a tilt variation of bedding slightly higher than 10º, and possibly, the latest variation occurs during the activity of the URS (Upper Riglos system) where the tilt variation of bedding is ca. 20º

(Fig. 13c).

Conclusions

New magnetostratigraphic data combined with the previous magnetostratigraphic data of Luesia section obtained in the continental deposits of the northern margin of the Ebro basin allow constraining the tectonic activity of the hinterland. The graphical summary represents with sketches in map view and cross sections the conclusions.

- A complete dating of the latest kinematics of the Pyrenean SW front is achieved, from syn-Gavarnie nappe activity (Broto and Fiscal basement thrust sheets) from 31.3 to 24.55 Ma, Rupelian-Chattian (Oligocene) to the syn-Guarga thrust activity, from 24.55 to 21.2 Ma Chattian-Aquitanian (Oligocene-Miocene).
- The latest tectonic activity in the frontal part of the Pyrenees is dated with the Uncastillo Fm, providing younger ages than previously assigned. Younger ages of ~ 5.4 ~1.5 and ~1.1 Myr are found for the beginning of the deformation connected to the Punta Común thrust sheet (from bottom of C10 to bottom of C6C, from 29.4 Ma to 24 Ma). Lower Riglos thrust sheet system (from C6C to C6B, from 24 to 22.5 Ma) and the Upper Riglos thrust system (from C6B to C6A, from 22.5 to 21.4 Ma) respectively.
- Accumulation rates at the northern margin of the basin vary and are related to the tectonic activity in the area: an increase in accumulation rate at 33.1 Ma within the interval of 26.1 to 53.9 cm/kyr occurs when the Gavarnie basement thrust ends its activity and Broto basement thrust starts its movement. A decrease in the accumulation rate at ~31.3 Ma to 34.9 cm/kyr coincides with the end of the Yebra de Basa cover thrust in the Jaca-Pamplona basin and the beginning of the San Felices cover thrust sheet in the External Sierras. At ~28 Ma, when the slowing down of the activity of the San Felices thrust sheet, a decrease in accumulation rate to 34.6 cm/kyr occurs. Variations in the accumulation rate with time of the Uncastillo Fm are related to the latest activity of the External Sierras. The larger accumulation rate occurs during the activity of Punta Común thrust sheet (39.3 cm/kyr).

  Smaller accumulation rates are recorded by younger deposits in the central part of the basin (TSU5 and 6), and are related to the different sedimentary environments (mostly carbonate and sulphate lacustrine), In the northern studied area the decrease in accumulation rate from an averaged of ~36 to less than 15 cm/kyr coincides with the boundary between TSU4 and 5 at ~21.9 Ma. The highest accumulation rates are in the northern margin of the Ebro basin in relation to alluvial-fluvial fans deposition, where accommodation space was larger due to the flexure of the lithosphere.

- Variations in the derivative of the accumulation rate respect to time also indicate the imprint of the cover and basement thrust in the area, particularly clear at the moment of closure of the basin to the sea ca. 36 Ma (beginning of the activity of the Yebra de Basa cover thrust), and at ca. 33 Ma (beginning of the activity of Broto basement thrust).

  The derivatives of the tilting variations show increases during the Punta Común thrust sheet and Upper Riglos thrust system. Tilting variation of bedding planes is larger during the Punta Común thrust sheet with ca. 40º (local unit U12) and during the Upper Riglos thrust system with ca. 20º.

Acknowledgements

Financial support was provided by the Spanish Ministry with the SEROS project, reference: CGL2014-55900-P / BTE and the project DR3AM- CGL2014-54118-C2-2-R. Thanks to the Paleomagnetic Laboratory CCiTUB-ICTJA CSIC, the Geomodels Research Institute, the *Grup de Geodinàmica i Anàlisi de Conques* - 2017SGR00596 and *Geotransfer* Group at the University of Zaragoza.

References

Allen, P.A., Homewood, P., Williams, G. D. 1986. Foreland basins: an introduction. In: Foreland Basins. Eds: P. A. Allen and P. Homewood, Special Publication of the International Association of Sedimentologists, 8, 3-12.

Arenas, C. 1993. Sedimentología y paleogeografía del Terciario del margen pirenaico y sector central de la Cuenca del Ebro (zona aragonesa occidental). Translated title: Tertiary sedimentology and paleogeography of the Pyrenean boundary and central sector of the Ebro basin (western aragonaise sector). Unpublished PhD Thesis, Faculty of Sciences, University of Zaragoza.

Arenas, C., Millán, H., Pardo, G., Pocoví, A. 2001. Ebro Basin continental sedimentation associated with late compressional Pyrenean tectonics (north-eastern Iberia): controls on basin margin fans and fluvial systems. Basin Res. 13, 65–89, doi.org/10.1046/j.1365-2117.2001.00141.x

Arenas, C. and Pardo, G. 1994. Estratigraffa del margen septentrional aragonés de la Cuenca del Ebro (sector Uncastillo-Bolea). Translated title: Stratigraphy of the northern aragonaise boundary of the Ebro basin (Uncastillo-Bolea sector). II Congreso del Grupo Español del Terciario.

Arenas, C., Pardo, G. 1999. Latest Oligocene–Late Miocene lacustrine systems of the north-central part of the Ebro Basin (Spain): sedimentary facies model and palaeogeographic synthesis. *Palaeogeography, Palaeoclimatology, Palaeoecology*, *151*(1-3), 127-148, doi.org/10.1016/S0031-0182(99)00025-5

Armitage, J.J., Duller, R.A., Whittaker, A.C. and Allen, P.A. 2011. Transformation of tectonic and climatic signals from source to sedimentary archive. *Nature Geoscience*, *4*(4), p.231.

Babault, J., Van Den Driessche, J., Bonnet, S., Castelltort, S., Crave, A. 2005. Origin of the highly elevated Pyrenean peneplain. *Tectonics*, *24*(2), doi.org/10.1029/2004TC001697

Barberà, X., Parés, J.M., Cabrera, L., Anadón, P. 1994. High-resolution magnetic stratigraphy across the Oligocene-Miocene boundary in an alluvial-lacustrine succession (Ebro Basin, northeast Spain). *Physics of the Earth and Planetary Interiors*, *85*(1-2), 181-193, doi.org/10.1016/0031-9201(94)90016-7

Barberà, X., Cabrera, L., Marzo, M., Parés, J.M., Agustí, J. 2001. A complete terrestrial Oligocene magnetobiostratigraphy from the Ebro Basin, Spain. *Earth and Planetary Science Letters*, *187*(1-2), 1-16, doi.org/10.1016/S0012-821X(01)00270-9

Beaumont, C. 1981. Foreland basins. *Geophysical Journal of the Royal Astronomical Society*, *65*(2), 291-329.

Beamud, E., Muñoz, J.A., Fitzgerald, P.G., Baldwin, S.L., Garcés, M., Cabrera, L., Metcalf, J.R. 2011. Magnetostratigraphy and detrital apatite fission track thermochronology in syntectonic conglomerates: constraints on the exhumation of the South-Central Pyrenees. *Basin Research*, *23*(3), 309-331, doi.org/10.1111/j.1365-2117.2010.00492.x

Bosch, G.V., Teixell, A., Jolivet, M., Labaume, P., Stockli, D., Domenech, M., Monie, P. 2016. Timing of Eocene–Miocene thrust activity in the Western Axial Zone and Chaînons Béarnais (west-central Pyrenees) revealed by multi-method thermochronology. *Comptes Rendus Géoscience*, *348*(3-4), 246-256.

Brunet M.F. 1986. The influence of the evolution of the Pyrenees on adjacent basins. Tectonophysics, 129, 343-354, doi.org/10.1016/0040-1951(86)90260-X

Burbank, D.W. Beck, R.A. 1991. Rapid, long-term rates of denudation. *Geology*, *19*(12), 1169-1172, doi.org/10.1130/0091-7613(1991)019<1169:RLTROD>2.3.CO;2

Burbank, D.W., Vergés, J., Muñoz, J.-A., Bentham, P. 1992. Coeval hindward and forward imbricating thrusting in the south-central Pyrenees, Spain: timing and rates of shortening and deposition. *GSA Bull.*104(1), 3-17, doi.org/10.1130/0016-7606(1992)104<0003:CHAFIT>2.3.CO;2

Calvín, P., Santolaria, P., Casas, A.M., Pueyo, E.L. 2018. Detachment fold vs. ramp anticline: a gravity survey in the southern Pyrenean front (External Sierras). *Geological Journal*, *53*(1), 178-190, doi.org/10.1002/gj.2884

Cámara, P. y Klimowitz, J. 1985. Interpretación geodinámica de la vertiente centro-occidental surpirenaica (cuencas de Jaca-Tremp). Translated title: Geodinamical interpretation of the west-central pyrenean sector (Jaca-Tremp basins). *Est. Geol.* 41: 391-404.

Cande, S.C., Kent, D.V. 1995. Revised calibration of the geomagnetic polarity timescale for the Late Cretaceous and Cenozoic. *Journal of Geophysical Research: Solid Earth*, *100*(B4), 6093-6095, doi.org/10.1029/94JB03098

Carroll, A.R., Chetel, L.M., Smith, M.E. 2006. Feast to famine: Sediment supply control on Laramide basin fill. *Geology*, *34*(3), 197-200, doi.org/10.1130/G22148.1

Casas, A., Kearey, P., Rivero, L., Adam, C.R. 1997. Gravity anomaly map of the Pyrenean region and a comparison of the deep geological structure of the western and eastern Pyrenees. *Earth and Planetary Science Letters*, *150*(1-2), 65-78, doi.org/10.1016/S0012-821X(97)00087-3

Chevrot, S., Sylvander, M., Diaz, J., Ruiz, M., Paul, A., PYROPE Working Group, 2014a. The Pyrenean architecture as revealed by teleseismic P-to-S converted waves recorded along two dense transects. *Geophysical Journal International*, *200*(2), 1096-1107, doi.org/10.1093/gji/ggu400.

Chevrot, S., Villaseñor, A., Sylvander, M., Benahmed, S., Beucler, E., Cougoulat, G., Delmas, P., Blanquat, M., Diaz, J., Gallart, J., Grimaud, F. 2014b. High-resolution imaging of the Pyrenees and Massif Central from the data of

the PYROPE and IBERARRAY portable array deployments. *Journal of Geophysical Research: Solid Earth*, *119*(8), 6399-6420, doi.org/10.1002/2014JB010953.

Choukroune, P., 1989. The ECORS Pyrenean deep seismic profile reflection data and the overall structure of an orogenic belt. *Tectonics*, *8*(1), 23-39, doi.org/10.1029/TC008i001p00023.

Costa, E., Garces, M., Lopez-Blanco, M., Beamud, E., Gomez-Paccard, M., Larrasoaña, J.C. 2010. Closing and continentalization of the South Pyrenean foreland basin (NE Spain): magnetochronological constraints. *Basin Research*, *22*(6), 904-917, doi.org/10.1111/j.1365-2117.2009.00452.x.

Costa, E., Garcés, M., Sáez, A., Cabrera, L., López-Blanco, M. 2011. The age of the "Grande Coupure" mammal turnover: New constraints from the Eocene–Oligocene record of the Eastern Ebro Basin (NE Spain). *Palaeogeography, Palaeoclimatology, Palaeoecology*, *301*(1-4), 97-107, doi.org/10.1016/j.palaeo.2011.01.005.

Curry, M. E., van der Beek, P., Huismans, R. S., Wolf, S.G., Muñoz, J.A. 2019. Evolving paleotopography and lithospheric flexure of the Pyrenean Orogen from 3D flexural modeling and basin analysis. *Earth and Planetary Science Letters*, 515, 26-37, doi.org/10.1016/j.epsl.2019.03.009.

DeCelles, P.G., Mitra, G. 1995. History of the Sevier orogenic wedge in terms of critical taper models, northeast Utah and southwest Wyoming. *Geological Society of America Bulletin*, *107*(4), 454-462, doi.org/10.1130/0016-7606(1995)107<0454:HOTSOW>2.3.CO;2

Densmore, A.L., Allen, P.A., Simpson, G. 2007. Development and response of a coupled catchment fan system under changing tectonic and climatic forcing. *Journal of Geophysical Research: Earth Surface*, *112*(F1). doi.org/10.1029/2006JF000474

Ford, M., Williams, E.A., Artoni, A., Vergés, J., Hardy, S. 1997. Progressive evolution of a fault-related fold pair from growth strata geometries, Sant Llorenc de Morunys, SE Pyrenees. *Journal of structural Geology*, *19*(3-4), 413-441, doi.org/10.1016/S0191-8141(96)00116-2

García-Castellanos, D., Vergés, J., Gaspar-Escribano, J., Cloetingh, S. 2003. Interplay between tectonics, climate, and fluvial transport during the Cenozoic evolution of the Ebro Basin (NE Iberia). *Journal of Geophysical Research: Solid Earth*, *108*(B7), doi.org/10.1029/2002JB002073

Gaspar-Escribano, J.M., van Wees, J.D., ter Voorde, M., Cloetingh, S., Roca, E., Cabrera, L. Muñoz, J.A., Ziegler, P.A., García-Castellanos. 2001. Three-dimensional flexural modelling of the Ebro Basin (NE Iberia). Geophysical Journal International, 145, 349-367, doi.org/10.1046/j.1365-246x.2001.01379.x

Gomis E. 1997. Precisión sobre la magnetoestratigrafía de las sucesiones del Oligoceno superior-Mioceno en los valles del Cinca, Segre y Ebro (sector SE de la Cuenca del Ebro, Provincias de Lleida, Zaragoza y Huesca). Translated title: Precission on the magnetostratigraphy of the upper Oligocene – Miocene in the Cinca, Segre and Ebro valleys (SE sector of the Ebro basin, Lleida, Zaragoza and Huesca provinces). Master thesis, Barcelona University 92.

Gomis E., Parés J.M., Cabrera L. 1999. Nuevos datos magneto-estrátigraficos del tránsito Oligoceno-Mioceno en el sector SE de la Cuenca del Ebro (provincias de Lleida, Zaragoza y Huesca, NE de España). Translated title: New magnetostratigraphic data of the Oligo-Miocene boundary in the SE sector of the Ebro basin (Lleida, Zaragoza and Huseca provinces, NE Spain). Acta Geol. Hisp. 32, 185-199.

Gunnell, Y., Calvet, M. 2006. Comment on "Origin of the highly elevated Pyrenean peneplain" by Julien Babault, Jean Van Den Driessche, and Stéphane Bonnet, Sébastien Castelltort, and Alain Crave. *Tectonics*, *25*(3), doi.org/10.1029/2005TC001849

Heermance, R.V., Chen, J., Burbank, D.W., Wang, C. 2007. Chronology and tectonic controls of Late Tertiary deposition in the southwestern Tian Shan foreland, NW China. *Basin Research*, *19*(4), 599-632, doi.org/10.1111/j.1365-2117.2007.00339.x

Hirst, J.P.P., Nichols, G.J. 1986. Thrust tectonic controls on Miocene alluvial distribution patterns, southern Pyrenees. In: Allen, P.A. and Homewood, P. (Eds.), *Foreland basins*, Int. Ass. Sediment. Spec. Publ., 8, 247-258.

Hogan, P.J., Burbank, D.W.,1996. Evolution of the Jaca piggyback basin and emergence of the External Sierra, southern Pyrenees. *Tertiary basins of Spain: the stratigraphic record of crustal kinematics*, *6*, p.153.

Huyghe, D., Mouthereau, F., Emmanuel, L. 2012. Oxygen isotopes of marine mollusc shells record Eocene elevation change in the Pyrenees. *Earth and Planetary Science Letters*, *345*, 131-141, doi.org/10.1016/j.epsl.2012.06.035

Izquierdo-Llavall, E., Aldega, L., Cantarelli, V., Corrado, S., Gil-Peña, I., Invernizzi, C., Casas, A.M. 2013. On the origin of cleavage in the Central Pyrenees: structural and paleo-thermal study. *Tectonophysics*, *608*, 303-318, doi.org/10.1016/j.tecto.2013.09.027

Jolivet, M., Labaume, P., Monié, P., Brunel, M., Arnaud, N., Campani, M. 2007. Thermochronology constraints for the propagation sequence of the south Pyrenean basement thrust system (France-Spain). *Tectonics*, *26*(5), doi.org/10.1029/2006TC002080

Jones, M. A., Heller, P.L., Roca, E., Garcés, M., Cabrera, L. 2004. Time lag of syntectonic sedimentation across an alluvial basin: theory and example from the Ebro Basin,Spain. *Basin Research*, 16, 467-488, doi.org/10.1111/j.1365-2117.2004.00244.x

Jordan, T.E. 1981. Thrust loads and foreland basin evolution, Cretaceous, western United States. *AAPG bulletin*, *65*(12), 2506-2520. Doi: 10.1306/03B599F4-16D1-11D7-8645000102C1865D

Karner, G.D., Watts, A.B. 1983. Gravity anomalies and flexure of the lithosphere at mountain ranges. J. Geophys. Res., 88: 10449-10477, doi: 10.1029/JB088iB12p10449

Kirschvink, J.L. 1980. The least-squares line and plane and the analysis of palaeomagnetic data. Geophysical Journal of the Royal Astronomical Society 62 (3), 699-718, doi.org/10.1111/j.1365-246X.1980.tb02601.x

Labaume, P.; Séguret, M., Seyve, C. 1985. Evolution of a turbiditic foreland basin an analogy with an accretionary prism: Example of the Eocene South-Pyrenean basin. *Tectonics.* 4 (7): 661-685, doi.org/10.1029/TC004i007p00661

Labaume, P., Meresse, F., Jolivet, M., Teixell, A., Lahfid, A. 2016. Tectonothermal history of an exhumed thrust-sheet-top basin: An example from the south Pyrenean thrust belt. *Tectonics*, *35*(5), 1280-1313, doi.org/10.1002/2016TC004192

Labaume, P., Teixell, A. 2018, 3D structure of subsurface thrusts in the eastern Jaca Basin, southern Pyrenees: Geologica Acta, v. 16, p. 477–498, doi: 10.1344/GeologicaActa2018.16.4.9, http://dx.doi.org/10.1344/GeologicaActa2018.16.4.9

Lanaja, J.M. 1987. Contribución de la Exploración Petrolífera Al Conocimiento de la Geología de España. Translated title: Contribution of the Oil Exploration to the Knowledge of the Geology in Spain. Publ. IGME, Madrid

Larrasoaña, J.C., Murelaga, X. and Garcés, M., 2006. Magnetobiochronology of Lower Miocene (Ramblian) continental sediments from the Tudela formation (western Ebro basin, Spain). *Earth and Planetary Science Letters*, *243*(3-4), 409-423.

Li, J., Fang, X., Song, Ch., Pan, B., Ma, Y., Yan, M. 2011. Quaternary rapid stepwise uplift of the NE Tibetan Plateau and its effects on climatic and environmental changes. Quaternary Research 81, 400-423, doi.org/10.1016/j.yqres.2014.01.002

Lowrie, W. 1990. Identification of ferromagnetic minerals in a rock by coercivity and unblocking temperature properties. *Geophysical research letters*, *17*(2), 159-162, doi.org/10.1029/GL017i002p00159

Luzón, A., González, A., Muñoz, A., Sánchez-Valverde, B. 2002. Upper Oligocene-Lowe Miocene shallowing-upward lacustrine sequences controlled by periodic and non-periodic processes (Ebro Basin, northeastern Spain). J. Palaeolimnology, 28, 441-456.

Luzón, A. 2005. Oligocene–Miocene alluvial sedimentation in the northern Ebro Basin, NE Spain: tectonic control and palaeogeographical evolution. Sediment. Geol. 177, 19–39, doi: 10.1016/j.sedgeo.2005.01.013

McElroy, R. 1990. Thrust kinematics and syntectonic sedimentation: the Pyrenean frontal ramp, Huesca, Spain. PhD Thesis. University of Cambridge, 175

Meigs, A.J. and Burbank, D.W., 1997. Growth of the South Pyrenean orogenic wedge. *Tectonics*, *16*(2), 239-258.

Millán-Garrido, H., Pocoví-Juan, A., Casas-Sainz, A.M. 1995a. El frente cabalgamiento surpirenaico en el extremo occidental de las Sierras Exteriores. Translated title: The South Pyrenean Frontal thrust in its western termination of the External Sierras. *Revista de la Sociedad Geológica de España*, *8*(1-2), 73-90.

Millán, H., Den Bezemer, T., Vergés, J., Marzo, M., Muñoz, J.A., Roca, E., Cirés, J., Zoetemeijer, R., Cloetingh, S., Puigdefàbregas, C., 1995b. Palaeo-elevation and effective elastic thickness evolution at mountain ranges: inferences from flexural modelling in the Eastern Pyrenees and Ebro Basin. *Marine and Petroleum Geology*, *12*(8), 917-928, doi.org/10.1016/0264-8172(95)98855-Y

Millán-Garrido, H., Pueyo-Morer, E., Aurell-Cardona, M., Luzón-Aguado, A., Oliva-Urcia, B., Martínez-Peña, B., 2000. Actividad tectónica registrada en los depósitos terciarios del frente meridional del Pirineo central. Translated title: Tectonic activity recorded in the tertiary deposits of the southern front of the central Pyrenees. *Revista de la Sociedad Geológica de España*, *13*(2), 279-300.

Molnar, P., 2001. Climate change, flooding in arid environments, and erosion rates. *Geology*, *29*(12), 1071-1074, doi.org/10.1130/0091-7613(2001)029<1071:CCFIAE>2.0.CO;2

Molnar, P., 2004. Late Cenozoic increase in accumulation rates of terrestrial sediment: How might climate change have affected erosion rates? *Annu. Rev. Earth Planet. Sci.*, *32*, 67-89, /doi.org/10.1146/annurev.earth.32.091003.143456

Morris, R.G., Sinclair, H.D. and Yelland, A.J. 1998. Exhumation of the Pyrenean orogen: implications for sediment discharge. *Basin Research*, *10*(1), 69-85, doi.org/10.1046/j.1365-2117.1998.00053.x

Muñoz, A., Arenas, C., González, A., Luzón, A., Pérez, A., Villena, J., Pardo, G. 2002, Ebro Basin (northeastern Spain), in Moreno, T., and Gibbons, W., eds., Geology of Spain: Geological Society of London, p. 301–334.

Muñoz, J.A., 1992. Evolution of a continental collision belt: ECORS-Pyrenees crustal balanced cross-section. In *Thrust tectonics* (235-246). Springer, Dordrecht.

Muñoz, J.A. Mencos, J. Roca, E. Carrera, N. Gratacós, O. Ferrer, O. Fernández, O. 2018. The structure of the South-Central Pyrenean fold and thrust belt as constrained by subsurface data. Geologica Acta, v. 16, p. 439–460, doi: 10.1344/GeologicaActa2018.16.4.7, http://dx.doi.org/10.1344/GeologicaActa2018.16.4.7

Ogg, J.G., 2012. Geomagnetic polarity time scale. In *The geologic time scale* (85-113).

Ogg, J.G., Ogg, G. and Gradstein, F.M., 2016. *A concise geologic time scale: 2016.* Elsevier.

Oliva-Urcia, B., Casas, A. M., Pueyo, E. L., Pocoví Juan, A. 2012. Structural and paleomagnetic evidence for non-rotational kinematics of the South Pyrenean Frontal Thrust at the western termination of the External Sierras (southwestern central Pyrenees). Geologica Acta, 10(2): 125-144, http://dx.doi.org/10.1344/105.000001704

Oliva-Urcia, B., Beamud, E., Garcés, M., Arenas, C., Soto, R., Pueyo, E. L., & Pardo, G. 2016. New magnetostratigraphic dating of the Palaeogene syntectonic sediments of the west-central Pyrenees: tectonostratigraphic implications. From: Pueyo, E. L., Cifelli, F., Sussman, A. J. & Oliva-Urcia, B. (eds) Palaeomagnetism in Fold and Thrust Belts: New Perspectives. Geological Society, London, Special Publications, 425, 107-128. http://doi.org/10.1144/SP425.5, updated version # 2015.

Oliva-Urcia, B. 2018 Thirty years (1988-2018) of advances in the knowledge of the structural evolution of the south-central Pyrenees during the Cenozoic collision, a summary. Revista de la Sociedad Geológica de España, 31 (2): 51-68.

Ori, G.G., Friend, P.F. 1984. Sedimentary basins formed and carried piggyback on active thrust sheets. *Geology*, *12*(8), 475-478.

Pardo, G., Villena, J., González, A. 1989. Contribución a los conceptos y a la aplicación del análisis tectosedimentario. Rupturas y unidades tectosedimentarias como fundamento de correlaciones estratigráficas. Translated title: Contributions to the concepts and application of tectosedimentary analyses. Ruptures and tectosedimentary units as the foundation for stratigraphic correlations. In: División de Unidades Estratigráficas en el Análisis de Cuencas (ed. by J. A. Vera), Rev. Soc. Geol. Esp., 2 (3-4), 199-221.

Pardo, G., Arenas, C., González, A., Luzón, A., Muñoz, A., Pérez, A., Pérez-Rivarés, F.J., Vázquez-Urbez, M., Villena, J. 2004. La cuenca del Ebro. Translated title: The Ebro basin. *Geología de España*, 533-543.

Paul, H.A., Zachos, J.C., Flower, B.P., Tripati, A. 2000. Orbitally induced climate and geochemical variability across the Oligocene/Miocene boundary. *Paleoceanography*, *15*(5), 471-485, doi.org/10.1029/1999PA000443

Peizhen, Z., Molnar, P., Downs, W.R. 2001. Increased sedimentation rates and grain sizes 2–4 Myr ago due to the influence of climate change on erosion rates. *Nature*, *410*(6831), p.891.

Pérez, A., Muñoz, A.;,Pardo, G., Villena, J., Arenas, C. 1988. Las unidades tectosedimentarias del Neógeno del borde ibérico de la Depresión del Ebro (sector central). Translated title: The tectosedimentary units of the Neogene in the Iberian range boundary of the Ebro basin. En: Sistemas lacustres neógenos del margen ibérico de la Cuenca del Ebro (Pérez, A.; Muñoz, A. y Sánchez, J.A, Ed.s), vol 1, 7-20, Secretariado de Publicaciones de la Universidad de Zaragoza.

Pérez-Rivarés, F.J., Garcés, M., Arenas, C., Pardo, G. 2002. Magnetocronología de la sucesión miocena de la Sierra de Alcubierre (sector central de la Cuenca del Ebro). Translated title: Magnetochronology of the Miocene succession of the Alcubierre Sierra. *Revista de la Sociedad Geológica de España*, *15*(3-4), 217-231.

Pérez-Rivarés. F.J., Pardo, G., Garcés, M., Arenas, C. 2003. Periodicidad sedimentaria en el registro lacustre de la Unidad Tectosedimentaria T6 de la sección de San Caprasio (Mioceno medio) del sector central de la Cuenca del Ebro. Translated title: Sedimentary periodicity in the lacustrine record of Tectosedimentary unit 6 in the San Caprasio section (middle Miocene) in the central sector of Ebro basin. Geotemas, 5, 195-198.

Pérez-Rivarés, F.J., Pardo-Tirapu, G.M., Arenas-Abad, M.C. and Garcés-Crespo, M. 2004. Magnetostratigraphy of the Miocene continental deposits of the Montes de Castejón (central Ebro basin, Spain): geochronological and paleoenvironmental implications. *Geologica Acta: an international earth science journal*, *2*(3), 221-234.

Pérez-Rivarés, F.J., Tirapu, G.M.P., Abad, M.C.A. and Crespo, M.G. 2004. Magnetostratigraphy of the Miocene continental deposits of the Montes de Castejón (central Ebro basin, Spain): geochronological and paleoenvironmental implications. *Geologica Acta: an international earth science journal*, *2*(3), 221-234, http://dx.doi.org/10.1344/105.000001429

Pérez-Rivarés, F.J., Arenas, C., Pardo, G. and Garcés, M. 2018. Temporal aspects of genetic stratigraphic units in continental sedimentary basins: Examples from the Ebro basin, Spain. *Earth-Science Reviews*, *178*, 136-153, doi.org/10.1016/j.earscirev.2018.01.019

Pocoví, A., Millán, H., Navarro, JJ., Martínez, M.B. 1990. Rasgos estructurales de la Sierra de Salinas y zona de los Mallos (Sierras Exteriores, Prepirineo, provincias de Huesca y Zaragoza). Translated title: Structural features of the Salinas Sierra and Mallos sector (External Sierras, Pre-Pyrenees, Huesca and Zaragoza provinces). *Geogaceta* 8. 36-39.

Pueyo, E.L., Millán, H., Pocoví, A. 2002. Rotation velocity of a thrust: a paleomagnetic study in the External Sierras (Southern Pyrenees). Sedimentary Geology, 146, 191 – 208, doi.org/10.1016/S0037-0738(01)00172-5

Puigdefàbregas, C., Muñoz, J.A. ,Vergés, J. 1992. Thrusting and foreland basin evolution in the southern Pyrenees. In *Thrust tectonics* (247-254). Springer, Dordrecht.

Puigdefàbregas, C. 1975. La sedimentación molásica en la cuenca de Jaca. Translated title: Molassic sedimentation in the Jaca basin. *Pirineos.* 104. 188

Quirantes, J. 1978. Estudio sedimentológico y estratigráfico del Terciario continental de los Monegros. Translated title: Sedimenological and stratigraphic study of the continental tertiary of Monegros region. Institución Fernando El Católico (CSIC), Diputación Provincial de Zaragoza, 200

Ramón, M. J., Pueyo, E. L., Oliva-Urcia, B., Larrasoaña, J. C. 2017. Virtual directions in paleomagnetism: A global and rapid approach to evaluate the NRM components. Frontiers in Earth Science, 5, 8, doi: 10.3389/feart.2017.00008

Riba, O. 1976. Syntectonic unconformities of the Alto Cardener, Spainish Pyrenees: A genetic interpretation. Sedimentary Geology, 15, 213-233. DOI: 10.1016/0037-0738(76)90017-8

Riba, O., Reguant, S. and Villena, J. 1983. Ensayo de síntesis estratigráfica y evolutiva de la cuenca terciaria del Ebro. Translated title: Stratigraphic and development synthesis essay of the Ebro tertiary basin. *Geologica España*, *2*, 131-159.

Rodríguez-Pintó, A., Ramón, M.J., Oliva-Urcia, B., Pueyo, E.L., Pocoví, A. 2011. Errors in paleomagnetism: Structural control on overlapped vectors–mathematical models. *Physics of the Earth and Planetary Interiors*, *186*(1-2), 11-22, doi.org/10.1016/j.pepi.2011.02.003

Roigé, M., Gómez-Gras, D., Remacha, E., Daza, R., Boya, S. 2016. Tectonic control on sediment sources in the Jaca basin (Middle and Upper Eocene of the South-Central Pyrenees). *Comptes Rendus Geoscience*, *348*(3-4), 236-245, doi.org/10.1016/j.crte.2015.10.005

Roure, F., Choukroune, P., Berastegui, X., Munoz, J.A., Villien, A., Matheron, P., Bareyt, M., Seguret, M., Camara, P., Deramond, J. 1989. ECORS deep seismic data and balanced cross sections: Geometric constraints on the evolution of the Pyrenees. *Tectonics*, *8*(1), 41-50, doi.org/10.1029/TC008i001p00041

Schlunegger, F., Jordan, T.E., Klaper, E.M. 1997. Controls of erosional denudation in the orogen on foreland basin evolution: the Oligocene central Swiss Molasse Basin as an example. *Tectonics*, *16*(5), 823-840, doi.org/10.1029/97TC01657

Teixell, A., García-Sansegundo, J. 1995. Estructura del sector central de la Cuenca de Jaca (Pirineos meridionales). Translated title: Structure of the central sector of the Jaca Basin (southern Pyrenees). *Rev. Soc. Geol. España.* Vol 8(3): 215-228.

Valero, L., Garcés, M., Cabrera, L., Costa, E., Sáez, A., 2014. 20 Myr of eccentricity paced lacustrine cycles in the Cenozoic Ebro Basin. Earth and Planetary Science Letters, 408, 183-193, doi.org/10.1016/j.epsl.2014.10.007

Vázquez-Úrbez, M., Arenas, C., Pardo, G., Pérez-Rivarés, J. 2013. The effect of Drainage Reorganization and Climate On the Sedimentologic Evolution of Intermontane Lake Systems: The Final Fill Stage of the Tertiary Ebro Basin (Spain). Journal of Sedimentary Research, 83 (8): 562-590, doi: 10.2110/jsr.2013.47

Vergés, J., Fernàndez, M., Martínez, A. 2002. The Pyrenean orogen: pre-, syn-, and post-collisional evolution. *Journal of the Virtual Explorer*, *8*, 55-74, doi:10.3809/jvirtex.2002.00058

Villena, J., Pardo, G., Pérez, A., Muñoz, A., González, A. 1996. The Tertiary of the Iberian margin of the Ebro basin: sequence stratigraphy. *Tertiary basins of Spain: the stratigraphic record of crustal kinematics*, (ed. by P. Friend & C. J. Dabrio), *6*, p.77-82. Cambridge University Press, Cambridge.

Willett, S.D., Schlunegger, F. 2010. The last phase of deposition in the Swiss Molasse Basin: From foredeep to negative-alpha basin. *Basin Research*, *22*(5), 623-639, doi.org/10.1111/j.1365-2117.2009.00435.x

Yuste, A., Luzón, A., Bauluz, B. 2004. Provenance of Oligo–Miocene alluvial and fluvial fans of the northern Ebro Basin (Spain): a XRD, petrographic and SEM study. Sediment. Geol. 172, 251–268, doi: 10.1016/j.sedgeo.2004.10.001

Zachos, J.C., Shackleton, N.J., Revenaugh, J.S., Pälike, H., Flower, B.P., 2001a. Climate response to orbital forcing across the Oligocene-Miocene boundary. *Science*, *292*(5515), 274-278, doi: 10.1126/science.1058288

Zachos, J., Pagani, M., Sloan, L., Thomas, E., Billups, K. 2001b. Trends, rhythms, and aberrations in global climate 65 Ma to present. Science, *292*(5517), 686-693, 10.1126/science.1059412

Zheng, H. Powell, ChM c, An, Z., Zhou, J, Don, G. 2000. Pliocene uplift of the northern Tibetan Plateau. Geology, 28 (8), 715-718, doi.org/10.1130/0091-7613(2000)28<715:PUOTNT>2.0.CO;2

Zheng, H., Huang, X., Butcher, K. 2006. Lithostratigraphy, petrography and facies analysis of the Late Cenozoic sediments in the foreland basin of the West Kunlun. *Palaeogeography, Palaeoclimatology, Palaeoecology*, *241*(1), 61-78, doi.org/10.1016/j.palaeo.2006.06.015

Zoetemeijer, R., Desegaulx, P., Cloetingh, S., Roure, F., Moretti, I. 1990. Lithospheric dynamics and tectonic-stratigraphic evolution of the Ebro Basin. Journal of Geophysical Research, 95(B3), 2701. doi:10.1029/jb095ib03p02701

Table 1. Paleomagnetic results from the Fuencalderas section. Site: name of the sample. Longitude and Latitude of the sample site. Level: thickness (m) from the bottom sample. Dg. Ig: declination and inclination in sample reference system; Ds. Is: declination and inclination in situ. Plat: paleolatitude. Int: intensity of the component. Error of the calculated component (which is MAD: maximum angular deviation). Q: quality of the component (1: good to 3: bad). T steps: number of temperature steps used for the calculation of the component. T range: temperature range over which component was calculated. *Characteristic component is calculated without including the origin. The grey shading indicates samples with Q ≥ 3.

site	LONGITUDE (W)	LATITUDE (N)	LEVEL (m)	Dg	Ig	Ds	Is	latp	int	err	Q	Trange	comment
FU04-2A	0° 52' 33.1320"	42° 23' 6.5796"	0	18.06	60.02	211.92	-5.32	-41.04	343.78	1.82	2	5	370-580
FU05-3B	0° 52' 34.4172"	42° 23' 5.7084"	18	3.39	76.51	213.17	-22.52	-47.85	303.61	6.78	2	4	* 250-490
FU06-2A	0° 52' 35.6916"	42° 23' 5.2224"	36	262.68	-40.64	24.23	9.79	46.71	361.96	4.44	2	6	520-680
FU07-1A	0° 52' 36.6492"	42° 23' 5.0208"	40.5	328.03	-52.99	345.31	40.53	67.12	420.61	4.06	2	6	450-680
FU08-2B	0° 52' 37.1892"	42° 23' 4.3548"	52.5	275.56	-47.51	350.70	7.66	50.47	280.23	4.84	2	5	290-520 (330out)
FU09-1A	0° 52' 37.9236"	42° 23' 3.9192"	64.5	312.43	-76.60	13.84	32.14	62.3	299.67	4.41	2	6	450-640
FU10-2A	0° 52' 38.5752"	42° 23' 3.4944"	79.5	281.61	-47.36	348.20	10.92	51.56	326.95	3.23	2	4	370-450
FU11-1A	0° 52' 39.0900"	42° 23' 3.0696"	87.5	336.42	5.33	273.67	28.29	12.77	237.28	9.00	2	6	550-680
FU12-2A	0° 52' 39.9612"	42° 23' 2.4072"	105.5	254.30	-18.42	341.54	-25.03	31.83	453.86	4.37	2	5	450-580
FU13-1B	0° 52' 41.3436"	42° 23' 1.1904"	132.5	168.49	67.60	194.97	-55.10	-76.53	1508.32	3.00	1	4	330-490
FU14-1A	0° 52' 41.7972"	42° 22' 59.6388"	163.5	331.22	38.09	288.46	-22.67	5.19	150.58	8.68	2	6	410-640
FU15-1A	0° 52' 42.3804"	42° 22' 58.9836"	180	182.58	75.78	211.00	-57.86	-66.23	2758.46	2.13	1	6	330-680
FU16-2A	0° 52' 43.3164"	42° 22' 58.8252"	196.5	91.93	66.94	214.01	-30.91	-51.19	669.44	5.79	1	6	370-640
FU500-1A	0° 52' 45.5520"	42° 22' 58.1952"	215	194.40	61.33	201.06	-30.59	-58.35	434.77	7.84	1	6	560-650
FU17-2A	0° 52' 46.0920"	42° 22' 57.7596"	231	219.21	54.16	216.66	-38.20	-52.91	495.76	2.52	2	3	290-370
FU501-1A	0° 52' 46.0308"	42° 22' 57.4392"	239.8	167.40	64.18	191.05	-21.77	-57.34	249.16	6.94	2	4	300-440
FU502-1A	0° 52' 46.8768"	42° 22' 57.1692"	259.5	328.58	32.34	262.28	22.63	2.34	321.37	1.78	2	5	440-500
FU503-1A	0° 52' 47.3160"	42° 22' 56.8560"	270	323.62	-14.60	313.97	24.28	40.39	265.31	5.49	2	5	500-530
FU504-1A	0° 52' 47.4168"	42° 22' 56.5824"	277.5	316.35	-12.12	312.54	16.21	36.19	257.56	4.03	2	4	350-470
FU505-1B	0° 52' 47.9280"	42° 22' 56.4204"	288	334.31	-5.06	306.85	34.61	39.67	283.53	2.85	2	5	350-500
FU20-2A	0° 52' 49.1736"	42° 22' 55.9380"	312	88.59	59.56	182.24	16.77	-38.89	359.02	6.83	2	5	290-520
FU506-2A	0° 52' 48.7452"	42° 22' 55.4520"	324	13.23	-17.48	350.82	64.90	82.16	403.39	4.23	2	5	350-560
FU507-1B	0° 52' 48.6696"	42° 22' 54.5628"	347	159.66	67.33	191.79	-12.55	-52.37	390.53	5.28	2	5	300-590
FU22-1A	0° 52' 48.6048"	42° 22' 54.0264"	360.5	202.16	40.67	201.38	-46.84	-67.47	744.71	3.84	1	6	290-660
FU508-2B	0° 52' 48.9108"	42° 22' 53.9508"	366.2	266.60	53.45	240.91	-17.07	-27.18	70.11	13.70	2	5	* 300-500
FU23-2A	0° 52' 49.1844"	42° 22' 53.7060"	377	14.78	-32.07	8.49	53.26	79.05	324.75	2.06	2	4	290-450
FU24-2A	0° 52' 49.2780"	42° 22' 53.1372"	393.5	204.26	41.92	203.91	-45.84	-65.3	860.44	3.09	1	6	290-680
FU510-1A	0° 52' 49.2024"	42° 22' 52.8924"	400.25	151.83	28.94	153.42	-26.96	-53.67	102.98	14.78	2	5	350-560
FU25-1A	0° 52' 49.2168"	42° 22' 52.5756"	405.5	205.11	18.16	197.91	-69.43	-74.05	372.56	1.59	2	4	370-450
FU511-1A	0° 52' 49.1988"	42° 22' 52.1976"	419	184.46	39.13	182.86	-42.96	-72.31	210.81	10.90	2	6	350-650
FU26-2A	0° 52' 49.1340"	42° 22' 52.0032"	423.5	201.37	18.89	189.18	-67.70	-79.72	144.81	5.91	2	3	290-370
FU512-1A	0° 52' 49.4868"	42° 22' 51.8088"	433.3	184.65	42.30	185.40	-40.42	-70.05	1171.76	2.85	1	6	300-620
FU27-2A	0° 52' 49.7388"	42° 22' 51.1788"	447.5	260.59	74.93	221.11	-7.40	-36.74	177.40	8.63	2	5	490-580
FU513-2	0° 52' 49.7100"	42° 22' 50.8692"	458	27.27	-67.21	28.46	20.78	49.71	47.36	6.64	2	4	350-440
FU28-1B	0° 52' 49.6992"	42° 22' 50.4948"	462.7	2.30	-5.76	341.29	71.86	71.4	236.83	7.36	2	5	330-550

FU29-2A	0° 52' 49.9152"	42° 22' 50.0196"	476.2	332.62	-13.52	312.09	44.98	48.08	144.96	10.62	2	6	520-660
FU515-1A	0° 52' 50.1240"	42° 22' 49.9368"	482.2	111.43	-2.45	100.62	-10.40	-11.37	883.70	3.89	2	6	530-620
FU516-1A	0° 52' 50.4336"	42° 22' 49.6128"	491.2	321.97	37.92	240.53	37.81	-5.38	248.91	7.38	2	6	500-590
FU30-1A	0° 52' 50.3580"	42° 22' 49.1952"	500.2	260.67	54.44	224.34	-3.47	-33.2	232.52	6.41	2	5	330-550
FU31-1A	0° 52' 50.3976"	42° 22' 49.0800"	506.2	191.72	28.07	191.90	-51.93	-76.31	121.41	12.57	2	4	330-490
FU32-1A	0° 52' 50.1060"	42° 22' 49.0008"	512.2	177.32	17.11	164.18	-59.57	-77.98	248.63	6.43	2	5	290-550
FU33-1A	0° 52' 49.9836"	42° 22' 48.6768"	518.2	160.12	51.11	170.59	-23.19	-58.51	184.30	6.27	2	4	250-490
FU34-1B	0° 52' 49.5228"	42° 22' 47.9928"	533.2	1.94	35.49	208.33	63.12	0.72	437.93	5.25	2	5	330-580
FU35-2A	0° 52' 49.4328"	42° 22' 47.8524"	539.2	279.98	62.79	218.82	8.28	-31.59	120.43	4.64	2	5	410-520
FU36-1A	0° 52' 49.3932"	42° 22' 47.5932"	545.2	198.44	66.71	194.19	-13.11	-52.01	76.95	22.86	2	4	* 250-410
FU37-1A	0° 52' 49.2060"	42° 22' 47.3268"	552.7	184.63	69.94	188.98	-9.92	-51.66	121.25	13.21	2	4	250-410
FU38-2A	0° 52' 48.9936"	42° 22' 47.0856"	558.7	217.77	70.56	199.91	-7.45	-47.38	224.32	11.53	2	9	330-520
FU39-1A	0° 52' 49.0116"	42° 22' 46.8228"	564.7	175.85	36.06	174.53	-41.69	-70.96	227.79	5.04	1	6	250-680
FU41-1A	0° 52' 48.5616"	42° 22' 46.1208"	578.2	218.33	42.08	214.82	-32.33	-51.34	187.89	10.82	2	5	290-580
FU42-1A	0° 52' 48.3348"	42° 22' 45.8796"	584.2	200.95	19.20	209.37	-59.29	-67.92	2327.63	1.98	1	6	290-680
FU44-1A	0° 52' 48.4140"	42° 22' 45.2604"	599.2	164.64	8.47	135.24	-57.67	-56.05	101.79	8.25	2	5	410-580
FU45-1A	0° 52' 48.3204"	42° 22' 45.1524"	604.2	134.46	30.40	140.09	-22.13	-43.54	155.24	10.96	2	3	250-330
FU46-1A	0° 52' 48.2340"	42° 22' 44.8644"	610.2	244.59	58.11	216.72	-9.42	-40.15	565.23	4.49	1	6	250-660
FU47-1A	0° 52' 48.1836"	42° 22' 44.7240"	616.2	200.09	27.99	203.70	-51.07	-68.37	374.08	4.31	2	5	290-580
FU48-2A	0° 52' 48.0504"	42° 22' 44.5116"	619.2	239.59	35.04	234.10	-25.90	-35.41	175.40	8.40	2	5	410-550
FU53-1A	0° 52' 58.7748"	42° 22' 46.8228"	628.2	211.70	-24.06	211.70	-24.06	-49.41	387.19	4.07	2	5	330-580
FU49-2A	0° 52' 47.5464"	42° 22' 43.9968"	634.2	5.72	54.96	195.81	44.82	-19.55	151.33	9.32	2	5	370-580
FU55-1A	0° 52' 59.4588"	42° 22' 46.5096"	641.7	151.62	40.28	161.25	-21.96	-54.87	103.84	13.60	2	6	490-660
FU56-1A	0° 52' 59.3832"	42° 22' 46.2108"	647.7	257.71	36.04	243.98	-14.87	-24.18	115.75	9.51	2	4	290-490
FU50-1B	0° 52' 47.7156"	42° 22' 43.5468"	647.7	203.56	40.45	203.18	-38.29	-61.46	233.26	8.46	2	5	330-520
FU52-1A	0° 52' 47.5464"	42° 22' 43.0248"	659.7	167.24	55.09	176.93	-19.91	-57.65	312.94	4.82	2	5	290-520
FU60-1A	0° 52' 59.4696"	42° 22' 45.0912"	671.7	27.81	5.32	28.13	52.32	65.92	105.39	11.71	2	4	* 290-450
FU62-1A	0° 52' 59.6892"	42° 22' 44.4108"	683.7	345.00	1.25	333.27	33.76	57	192.57	11.54	2	4	250-450
FU63-1A	0° 53' 0.0852"	42° 22' 44.1840"	691.2	235.69	19.02	236.46	-22.71	-32.49	103.51	7.82	2	5	370-520
FU64-1A	0° 53' 0.3336"	42° 22' 43.7916"	700.2	196.67	18.53	196.06	-31.23	-60.93	517.57	6.37	2	5	370-580
FU66-2B	0° 53' 0.2184"	42° 22' 43.1832"	712.2	137.45	-17.64	114.18	-30.33	-28.65	57.77	4.21	2	4	330-410
FU87-1A	0° 53' 37.1184"	42° 22' 49.5300"	721.2	341.16	67.68	227.76	54.46	-1.06	107.96	8.81	2	6	250-580
FU67-1B	0° 53' 0.3372"	42° 22' 42.6180"	721.2	312.21	-11.07	313.71	7.62	33.61	153.33	12.37	2	5	290-580
FU68-2A	0° 53' 0.5784"	42° 22' 42.2760"	727.2	327.53	24.83	293.44	42.15	33.08	447.06	5.36	1	5	250-520
FU88-2A	0° 53' 37.2444"	42° 22' 49.6812"	727.4	345.59	27.05	304.03	57.06	47.68	221.78	6.96	2	6	410-610
FU89-1A	0° 53' 36.5640"	42° 22' 48.7236"	736.4	10.38	15.53	355.90	63.42	86.14	82.10	2.91	2	6	550-610
FU90-2A	0° 53' 36.1608"	42° 22' 48.4752"	742.1	17.29	12.64	11.74	62.29	81.36	278.36	4.45	2	6	330-610
FU71-2B	0° 53' 1.0248"	42° 22' 41.4732"	745.2	346.38	-4.51	337.02	34.60	59.54	268.44	11.57	2	6	250-610
FU92-1B	0° 53' 35.9520"	42° 22' 47.8992"	753.1	201.47	37.15	201.62	-12.84	-49.25	176.54	15.38	2	6	* 290-610
FU94-2A	0° 53' 35.2968"	42° 22' 47.3052"	766.3	179.75	-16.26	156.29	-59.22	-72.06	89.91	8.06	2	6	410-610
FU72-2A	0° 53' 2.1840"	42° 22' 40.6164"	769.2	182.21	13.02	178.55	-33.79	-65.97	493.65	4.06	2	5	290-490
FU95-2A	0° 53' 35.1204"	42° 22' 46.9524"	771.9	203.89	4.52	204.55	-45.46	-64.67	90.16	6.74	2	4	330-450
FU73-1A	0° 53' 1.9392"	42° 22' 40.2924"	775.2	176.79	-13.50	154.92	-55.31	-69.54	1191.74	2.33	1	6	330-640
FU96-1A	0° 53' 34.5984"	42° 22' 46.6284"	777.9	201.77	-1.68	201.45	-51.68	-70.24	1056.86	2.73	1	6	290-610
FU74-2A	0° 53' 2.0004"	42° 22' 39.8532"	781.2	178.27	-24.77	142.14	-64.77	-62.98	148.60	2.53	2	6	520-610
FU518-1B	0° 53' 34.8936"	42° 22' 46.1748"	784.5	189.54	36.36	191.44	-3.20	-47.84	586.46	5.49	2	5	530-590
FU75-1A	0° 53' 1.9824"	42° 22' 39.4428"	788.7	164.41	2.39	153.58	-35.25	-57.96	148.40	4.51	2	4	330-410

FU519-2A	0° 53' 34.6236"	42° 22' 45.7104"	790.4	207.56	-7.93	212.49	-37.99	-55.59	59.21	14.23	2	4	* 400-470
FU97-2A	0° 53' 34.4796"	42° 22' 45.8940"	790.4	191.09	16.97	191.07	-15.02	-53.8	80.36	12.24	2	5	250-490
FU98-2A	0° 53' 34.3788"	42° 22' 45.6024"	792.2	164.89	-50.55	116.53	-74.04	-48.58	210.94	8.47	2	2	250-490
FU98-1B	0° 53' 34.3788"	42° 22' 45.6024"	792.2	155.76	14.12	155.97	-12.79	-48.18	99.22	5.22	2	3	250-370 (300out)
FU76-1A	0° 53' 1.7520"	42° 22' 39.2736"	794.7	177.44	-0.76	166.04	-44.72	-70.21	295.33	10.54	2	5	330-640
FU99-2A	0° 53' 34.2312"	42° 22' 45.4368"	794.8	164.74	-1.37	160.59	-30.14	-58.89	178.14	4.98	2	3	250-370
FU100-1A	0° 53' 34.1556"	42° 22' 45.3792"	796.5	167.54	4.86	166.25	-17.41	-54.31	242.51	10.37	2	5	370-550
FU100-2A	0° 53' 34.1556"	42° 22' 45.3792"	796.5	155.69	-33.18	138.98	-50.57	-55.72	89.60	12.75	2	5	250-550
FU520-1	0° 53' 34.0620"	42° 22' 45.2676"	798.2	145.76	32.85	153.55	7.89	-37.72	91.12	9.07	2	5	400-500
FU101-2A	0° 53' 33.7488"	42° 22' 44.9184"	802.9	334.24	13.28	327.00	31.53	52.12	467.89	4.47	1	5	250-490 (290out)
FU101-1A	0° 53' 33.7488"	42° 22' 44.9184"	802.9	311.52	23.79	298.69	32.85	32.99	481.42	2.51	2	5	370-520
FU521-2	0° 53' 33.6660"	42° 22' 44.9508"	803.4	346.48	-17.82	347.84	4.50	48.31	169.60	5.48	2	5	440-530
FU102-2A	0° 53' 33.2628"	42° 22' 44.5620"	808.7	19.73	15.02	21.14	39.89	63.51	377.78	7.85	1	5	290-520
FU102-3A	0° 53' 33.2628"	42° 22' 44.5620"	808.7	165.92	50.58	174.38	27.65	-32.59	340.43	6.81	2	5	250-450
FU77-1A	0° 53' 1.6476"	42° 22' 38.5392"	809.7	299.70	-36.97	325.92	-17.93	29.67	479.06	7.49	2	5	410-550
FU103-1A	0° 53' 33.0396"	42° 22' 44.1984"	812	332.20	54.12	280.37	66.30	36.53	234.90	9.22	2	5	330-550
FU104-2A	0° 53' 32.7048"	42° 22' 43.8960"	814.7	320.88	69.56	239.46	65.94	14.73	226.92	9.69	2	5	330-490
FU78-2A	0° 53' 1.6836"	42° 22' 38.1792"	815.7	177.36	41.56	183.82	-5.35	-50.04	133.37	12.51	2	6	610-640
FU522-1	0° 53' 32.2368"	42° 22' 43.6296"	821.4	357.23	27.50	346.45	55.24	77.54	657.31	3.44	1	6	440-620
FU79-2A	0° 53' 2.1804"	42° 22' 37.7796"	823.2	14.64	6.96	8.53	56.25	81.32	314.19	3.18	2	6	640-660
FU105-2A	0° 53' 32.1468"	42° 22' 43.3236"	824.5	2.99	53.01	325.81	80.28	56.8	81.81	8.47	2	3	250-370 (290out)
FU523-1	0° 53' 32.1576"	42° 22' 43.1652"	827	171.45	1.13	168.54	-26.11	-59.61	130.99	13.58	2	5	* 350-530
FU80-1A	0° 53' 2.0976"	42° 22' 37.4160"	829.2	18.88	6.52	16.15	56.38	76.42	169.73	4.27	2	5	490-580
FU524-2	0° 53' 32.5356"	42° 22' 43.0068"	832.7	191.62	10.55	191.47	-19.39	-55.97	189.54	6.41	2	4	300-440
FU81-2B	0° 53' 2.1048"	42° 22' 37.0884"	833.7	15.65	18.06	5.71	67.33	81.43	227.93	4.95	2	6	550-610
FU83-2B	0° 53' 1.9176"	42° 22' 36.7572"	842.7	196.53	-31.27	172.32	-80.10	-61.49	671.75	3.81	2	6	330-640
FU106-1A	0° 53' 34.1196"	42° 22' 42.6864"	846.9	155.10	-52.75	105.65	-67.00	-40.07	205.70	3.47	2	4	250-410
FU106-2A	0° 53' 34.1196"	42° 22' 42.6864"	846.9	216.21	26.84	213.87	-1.47	-38.37	183.26	6.44	2	5	370-490
FU525-1A	0° 53' 34.1448"	42° 22' 42.7944"	846.9	142.10	-29.48	121.73	-43.39	-39.74	112.15	6.10	2	5	440-530
FU107-1A	0° 53' 35.4300"	42° 22' 42.6504"	854.2	196.91	-3.28	199.22	-39.88	-64.53	87.88	12.30	2	5	370-550
FU107-2A	0° 53' 35.4300"	42° 22' 42.6504"	854.2	174.99	-37.75	150.55	-71.81	-66.52	115.40	4.78	2	5	330-550
FU85-1A	0° 53' 2.2884"	42° 22' 35.8788"	860	178.70	21.33	178.04	-24.84	-60.48	184.69	7.24	2	6	410-640
FU526-1A	0° 53' 36.3840"	42° 22' 42.8988"	864.1	242.04	17.23	239.20	-6.40	-24.51	250.37	7.41	2	5	530-560
FU86-2A	0° 53' 3.0048"	42° 22' 35.8788"	865.95	183.28	6.80	177.31	-40.02	-70.15	360.82	3.45	2	5	330-490
FU108-1A	0° 53' 37.7052"	42° 22' 41.7036"	888.7	173.43	-23.88	160.71	-58.49	-75.07	125.66	4.61	2	4	290-410
FU527-1B	0° 53' 37.7340"	42° 22' 41.7648"	888.7	147.84	19.27	150.00	-9.33	-43.76	242.34	8.70	2	4	300-400
FU528-1	0° 53' 37.5432"	42° 22' 41.5596"	893.7	206.31	25.78	204.80	-9.84	-46.48	137.45	5.81	2	5	530-590
FU109-1A	0° 53' 37.5828"	42° 22' 41.0448"	900.4	160.61	-2.30	153.94	-34.02	-57.52	83.34	8.55	2	5	370-520
FU529-2	0° 53' 37.4712"	42° 22' 41.1276"	900.4	190.43	-11.15	190.96	-48.14	-74.01	247.88	6.43	2	5	300-560
FU110-1A	0° 53' 36.8484"	42° 22' 40.1340"	913.4	180.14	-0.39	176.73	-33.81	-65.85	172.42	8.98	2	4	370-450
FU110-2A	0° 53' 36.8484"	42° 22' 40.1340"	913.4	159.57	12.91	159.10	-15.37	-50.75	221.02	6.22	2	5	370-520
FU531-2	0° 53' 34.0656"	42° 22' 39.3816"	918.9	172.87	3.19	169.40	-28.68	-61.31	48.03	25.90	2	4	300-440
FU112-1A	0° 53' 33.7848"	42° 22' 39.2880"	920.4	348.35	21.01	333.34	50.06	65.79	114.17	7.11	2	4	290-450
FU532-2	0° 53' 33.5688"	42° 22' 38.8632"	927.4	9.64	-25.50	10.21	9.29	51.1	277.61	1.80	2	5	400-500
FU533-2	0° 53' 33.4428"	42° 22' 38.3880"	933.5	10.69	-2.57	9.67	32.24	63.68	413.87	2.32	2	5	300-530
FU114-1A	0° 53' 33.2484"	42° 22' 38.2548"	935	352.85	18.98	340.62	49.81	70.5	792.63	5.95	1	6	290-580
FU114-2A	0° 53' 33.2484"	42° 22' 38.2548"	935	351.95	26.54	334.41	56.46	69.67	702.29	4.00	2	5	290-520

FU534-1	0° 53' 33.4608"	42° 22' 37.8480"	942.9	61.05	-6.68	63.63	18.02	25.58	211.76	5.06	2	5	470-530
FU535-1	0° 53' 33.3816"	42° 22' 37.7652"	944.8	48.48	-18.02	47.48	12.02	34.54	143.98	5.81	2	4	350-470
FU115-2A	0° 53' 33.4284"	42° 22' 37.5348"	946.5	263.54	73.11	218.99	46.00	-11.44	312.61	2.72	2	4	290-450
FU537-1	0° 53' 34.2024"	42° 22' 36.8508"	959.8	337.26	-1.51	332.26	25.07	52.12	319.25	6.06	2	5	400-530
FU538-1B	0° 53' 34.2492"	42° 22' 36.8688"	961.1	297.27	31.44	313.59	19.52	38.2	256.95	5.82	2	5	350-590
FU539-2A	0° 53' 34.8792"	42° 22' 36.6060"	969.6	287.33	51.14	322.31	39.16	52.67	244.10	5.53	2	5	500-560
FU117-1A	0° 53' 35.2860"	42° 22' 35.0328"	996.6	101.21	-61.27	57.97	-43.93	3.38	155.17	12.92	2	6	450-610
FU542-1	0° 53' 35.1672"	42° 22' 34.8924"	1000.1	215.84	35.67	212.08	2.20	-37.71	360.60	5.85	2	5	300-560
FU118-1A	0° 53' 35.2032"	42° 22' 34.6368"	1000.7	163.23	-12.08	152.23	-39.90	-59.6	157.70	3.27	2	5	370-520
FU543-2	0° 53' 34.6272"	42° 22' 34.0140"	1014.7	201.32	40.21	200.15	5.30	-41.31	167.70	21.33	2	5	* 300-560
FU119-2A	0° 53' 34.3752"	42° 22' 33.8880"	1015.3	0.15	37.39	337.71	69.25	71.89	304.46	4.91	2	5	250-520
FU544-1	0° 53' 34.0944"	42° 22' 33.6720"	1016.6	322.68	42.86	283.00	53.76	31.18	159.35	10.25	2	4	300-400
FU545-1	0° 53' 33.8136"	42° 22' 33.5784"	1019.8	27.17	-52.16	23.27	-17.54	34.3	358.22	4.22	2	4	300-400
FU120-1A	0° 53' 33.7344"	42° 22' 33.3948"	1021.3	320.95	29.52	296.03	43.43	35.55	401.57	6.06	2	5	330-520
FU547-1	0° 53' 32.5896"	42° 22' 32.3580"	1031.2	312.64	33.25	285.50	41.45	26.94	405.25	3.77	2	5	300-500
FU122-1A	0° 53' 32.5320"	42° 22' 32.0628"	1034.7	1.64	40.39	348.19	59.56	80.91	179.31	4.59	2	4	250-490
FU548-2	0° 53' 32.1432"	42° 22' 31.4652"	1041.4	342.77	2.44	336.31	30.83	57.16	170.76	11.31	2	4	* 300-400
FU549-1	0° 53' 32.5896"	42° 22' 31.0836"	1047.4	312.87	0.56	308.27	15.34	32.97	388.26	3.32	2	4	350-400
FU550-1A	0° 53' 33.3384"	42° 22' 30.6192"	1055.9	338.41	58.29	303.81	70.92	52.09	256.48	6.93	2	5	500-560
FU125-1A	0° 53' 33.9900"	42° 22' 29.8560"	1070.9	190.13	31.70	191.50	2.01	-45.28	132.51	12.92	2	4	290-450
FU552-2A	0° 53' 33.8244"	42° 22' 28.9668"	1078.4	159.63	38.21	168.25	13.49	-39.51	132.00	9.35	2	5	440-500
FU126-3A	0° 53' 33.9540"	42° 22' 28.7652"	1080.9	5.81	7.10	2.64	36.12	67.44	116.09	7.54	2	5	330-520
FU127-2A	0° 53' 33.9432"	42° 22' 27.9588"	1090.1	1.18	25.83	351.14	53.62	79.16	61.97	7.80	2	5	330-520
FU128-2A	0° 53' 33.6516"	42° 22' 27.3756"	1098.1	143.31	-24.62	126.42	-37.95	-40.79	136.25	5.84	2	4	250-490
FU129-2A	0° 53' 33.6768"	42° 22' 26.7996"	1105.6	123.29	-2.14	120.41	-8.81	-25.11	179.23	7.09	2	4	370-490
FU131-1A	0° 53' 33.3420"	42° 22' 25.2228"	1121.1	190.29	-37.00	190.75	-57.00	-80.43	885.11	1.51	2	5	350-530
FU134-2B	0° 53' 32.2440"	42° 22' 24.2688"	1131.7	209.42	9.44	209.42	-9.37	-44.07	165.36	3.04	2	4	350-440
FU135-2A	0° 53' 31.7040"	42° 22' 24.3840"	1135.4	171.36	15.63	172.02	-3.45	-48.6	34.10	9.65	2	5	470-530
FU136-2A	0° 53' 31.2000"	42° 22' 23.6928"	1139.1	192.49	-15.62	193.08	-35.58	-64.66	73.86	10.48	2	5	350-560
FU137-1A	0° 53' 30.7644"	42° 22' 23.5200"	1142.4	193.25	-7.42	193.71	-27.37	-59.62	154.19	8.16	2	5	350-560
FU138-2A	0° 53' 30.4404"	42° 22' 23.0556"	1145.4	136.52	-14.82	130.27	-26.12	-38.59	341.03	3.63	2	5	350-500
FU139-2B	0° 53' 30.2640"	42° 22' 22.5912"	1148.7	327.25	51.58	301.01	63.38	48.25	91.53	5.85	2	4	350-470
FU140-1A	0° 53' 30.0444"	42° 22' 22.3896"	1151.3	348.28	50.11	331.83	67.78	69.13	77.00	11.51	2	4	350-440
FU141-1A	0° 53' 29.2416"	42° 22' 20.3880"	1161.3	303.51	24.84	293.28	31.47	28.44	32.52	7.60	2	4	470-530
FU142-1A	0° 53' 29.3136"	42° 22' 20.1972"	1162.3	29.04	-11.12	28.73	6.95	43.35	257.26	3.11	2	4	300-470
FU143-1B	0° 53' 29.9904"	42° 22' 19.4628"	1169.3	221.81	35.03	215.86	18.68	-28.46	223.03	7.56	2	5	500-590
FU144-1A	0° 53' 30.5952"	42° 22' 19.0596"	1172.3	124.94	57.94	143.97	44.52	-13.71	1029.84	2.76	2	4	300-400
FU145-1A	0° 53' 31.2000"	42° 22' 18.4188"	1177.3	167.18	34.70	169.61	15.35	-38.8	267.86	2.78	2	5	470-500
FU146-1A	0° 53' 32.7624"	42° 22' 16.1580"	1184.8	145.46	-31.82	140.83	-39.48	-51.79	193.06	4.35	2	5	400-500
FU147-1A	0° 53' 32.1684"	42° 22' 14.9304"	1190.8	210.29	11.96	209.70	3.02	-38.49	35.89	14.74	2	5	400-530
FU149-1B	0° 53' 29.9184"	42° 22' 11.3124"	1195.5	256.65	14.38	254.79	12.50	-6.77	418.89	4.22	2	5	300-560
FU150-1A	0° 53' 30.1128"	42° 22' 11.3556"	1197.5	210.54	-46.80	215.89	-53.45	-60.8	96.57	3.18	2	4	400-470
FU151-2A	0° 53' 29.4360"	42° 22' 10.4880"	1200.5	344.14	8.94	343.65	16.65	53.09	96.67	6.13	2	6	300-590
FU152-1A	0° 53' 30.4332"	42° 22' 11.1576"	1201.8	188.77	-0.28	188.86	-8.17	-50.8	297.53	3.68	2	5	350-560(470out)
FU153-2A	0° 53' 30.5844"	42° 22' 11.0244"	1203.8	163.37	-62.24	157.55	-69.82	-71.43	996.15	2.42	2	5	300-590(530out)
FU154-1A	0° 53' 30.9300"	42° 22' 10.8840"	1207	150.27	-50.80	144.39	-57.60	-62.74	157.14	15.37	2	5	* 300-560

FU155-1A	0° 53' 30.9552"	42° 22' 10.6968"	1210	335.54	49.22	330.90	56.42	67.07	129.60	30.76	2	5	* 470-560
FU157-1	0° 53' 27.1464"	42° 22' 7.5756"	1215.5	215.41	-39.74	220.03	-46.01	-54.29	84.32	24.96	2	4	* 350-470
FU160-1A	0° 53' 26.0340"	42° 22' 6.0996"	1226.3	219.61	17.93	218.25	11.76	-30.39	34.66	41.35	2	4	400-470
FU21-2B	0° 52' 48.4320"	42° 22' 54.7932"	338	99.17	7.72	126.79	20.21	-18.18	455.59	2.71	3	4	330-410
FU509-1A	0° 52' 49.0260"	42° 22' 53.5332"	383	156.25	-31.48	82.82	-32.04	-6.53	307.40	2.91	3	5	300-500
FU61-2A	0° 52' 59.4084"	42° 22' 44.7816"	677.7	349.60	-11.44	345.66	25.59	58.43	252.33	12.05	3	4	250-450
FU93-1A	0° 53' 35.6388"	42° 22' 47.6004"	760.8	210.30	33.81	209.21	-15.82	-47.05	123.04	18.86	3	6	640-660
FU104-1B	0° 53' 32.7048"	42° 22' 43.8960"	814.7	324.60	52.89	277.03	61.85	31.82	303.84	5.51	3	4	250-450
FU105-1A	0° 53' 32.1468"	42° 22' 43.3236"	824.5	89.92	23.32	104.46	27.69	-0.38	165.88	7.05	3	3	250-370
FU82-2A	0° 53' 1.9284"	42° 22' 37.0560"	836.7	137.90	14.60	140.18	-9.11	-38.2	92.02	8.37	3	6	580-610
FU84-2A	0° 53' 2.0112"	42° 22' 36.3432"	850.2	250.65	16.49	251.10	-17.80	-20.05	112.82	1.36	3	4	370-410
FU108-2A	0° 53' 37.7052"	42° 22' 41.7036"	888.7	161.75	-20.52	145.53	-51.23	-60.82	393.97	2.93	3	3	290-370 (330out)
FU109-2A	0° 53' 37.5828"	42° 22' 41.0448"	900.4	149.97	-6.33	140.30	-33.41	-48.62	195.08	6.77	3	4	330-450
FU530-2	0° 53' 36.6468"	42° 22' 40.2528"	913.4	159.56	30.41	165.23	1.04	-44.97	153.23	1.92	3	4	350-400
FU113-1A	0° 53' 33.5544"	42° 22' 38.5176"	929.4	41.52	11.61	50.66	42.31	44.85	289.46	9.02	3	4	330-410
FU113-2A	0° 53' 33.5544"	42° 22' 38.5176"	929.4	30.31	11.64	35.98	45.26	56.82	162.06	4.99	3	4	330-410
FU536-2B	0° 53' 33.8892"	42° 22' 36.9012"	958.1	114.43	6.23	116.52	0.48	-19.05	196.95	4.51	3	4	300-440
FU541-2	0° 53' 35.3580"	42° 22' 35.2056"	996.6	303.66	-17.31	310.22	-4.61	26.64	400.09	4.63	3	5	500-530
FU118-2A	0° 53' 35.2032"	42° 22' 34.6368"	1000.7	139.82	-8.22	130.20	-25.51	-38.29	277.84	6.46	3	4	330-410
FU546-1	0° 53' 33.0756"	42° 22' 32.8260"	1028.1	108.59	9.77	113.80	6.69	-14.92	144.82	9.29	3	4	350-400
FU122-2A	0° 53' 32.5320"	42° 22' 32.0628"	1034.7	356.76	9.42	352.89	28.45	61.98	127.28	6.52	3	2	200-250
FU123-2A	0° 53' 32.1144"	42° 22' 31.6128"	1039.9	348.44	-8.72	348.39	9.31	50.8	129.95	2.90	3	2	200-250
FU124-1A	0° 53' 33.7956"	42° 22' 30.3312"	1061.9	195.63	-46.87	196.61	-66.86	-76.55	46.83	19.13	3	2	150-250
FU125-2A	0° 53' 33.9900"	42° 22' 29.8560"	1070.9	259.66	34.99	247.46	17.10	-10.17	137.65	8.56	3	2	150-250
FU551-1	0° 53' 34.0476"	42° 22' 29.9532"	1070.9	234.45	51.74	222.52	25.27	-21.94	383.07	1.97	3	4	350-400
FU126-2A	0° 53' 33.9540"	42° 22' 28.7652"	1080.9	312.12	54.95	337.98	36.69	61.21	90.61	5.51	3	2	150-250
FU553-2A	0° 53' 33.8928"	42° 22' 28.2936"	1085.4	16.35	-58.41	17.55	-28.43	30.13	187.75	4.49	3	5	470-560
FU127-1A	0° 53' 33.9432"	42° 22' 27.9588"	1090.1	347.48	-24.54	350.63	1.54	47.43	188.17	3.00	3	2	150-250
FU128-1A	0° 53' 33.6516"	42° 22' 27.3756"	1098.1	5.16	36.27	351.98	64.58	83.05	109.39	4.56	3	2	* 150-250
FU554-1B	0° 53' 33.7128"	42° 22' 26.8824"	1105.6	231.14	17.30	229.92	-8.51	-31.59	80.03	4.29	3	3	250-300
FU129-1A	0° 53' 33.6768"	42° 22' 26.7996"	1105.6	123.77	-4.35	119.74	-10.97	-25.42	475.49	1.50	3	2	150-250
FU130-2A	0° 53' 33.6948"	42° 22' 26.0616"	1117.6	116.75	11.76	121.61	6.49	-20.33	337.37	4.66	3	2	150-250
FU132-1A	0° 53' 33.1872"	42° 22' 24.8556"	1124.3	281.90	23.75	273.14	23.12	10.4	539.36	10.47	3	6	620-650
FU159-1A	0° 53' 26.3688"	42° 22' 6.5928"	1224	252.89	-51.82	263.18	-53.39	-26.73	46.53	2.63	3	4	350-400
FU502-1A	0° 52' 46.8768"	42° 22' 57.1692"	259.5	200.68	-45.29	37.35	-41.11	15.49	236.39	13.64	4	4	* 250-400
FU503-1A	0° 52' 47.3160"	42° 22' 56.8560"	270	154.17	38.25	162.01	-28.74	-58.75	50.07	19.62	4	4	* 350-470
FU541-2	0° 53' 35.3580"	42° 22' 35.2056"	996.6	201.91	-41.55	213.97	-76.05	-61.29	79.38	30.40	4	4	* 250-470
FU132-1A	0° 53' 33.1872"	42° 22' 24.8556"	1124.3	157.48	10.63	157.87	-6.45	-46.05	327.35	23.05	4	5	* 250-590

Table 2. Paleomagnetic results from the San Marzal section. Elements as in Table 1

site	LONGITUDE (W)	LATITUDE (N)	LEVEL (m)	Dg	Ig	Ds	Is	latp	int	err	Q	Tran ge	comment
sm001-2a	0° 57' 52.76" W	42° 27' 53.01" N	0	301.44	-49.22	217.22	-38.57	-52.7	42.84	36.47	2	4	400-460
sm002-1a	0° 57' 52.8" W	42° 27' 53.16" N	3	296.04	-33.09	238.02	-36.34	-36.9	1069.47	4.00	2	3	*230-370
sm003-2a	0° 57' 53.35" W	42° 27' 53.23" N	6	306.18	-29.92	242.23	-44.98	-37.5	39.42	6.98	2	4	400-460
sm005-1a	0° 57' 53.2" W	42° 27' 53.43" N	13.5	183.59	-31.19	184.34	38.14	-26	251.96	12.14	2	5	* 340-550
sm006-2a	0° 57' 53.3" W	42° 27' 53.63" N	16.5	87.04	49.96	37.09	16.46	42.9	497.94	11.10	2	6	* 370-580
sm011-1a	0° 57' 53.42" W	42° 27' 54.14" N	31.25	161.30	40.93	21.12	66.03	74.1	169.98	9.43	2	3	300-370
sm014-2a	0° 57' 53.78" W	42° 27' 54.62" N	44.25	162.69	52.04	36.99	51.55	59.1	78.95	9.56	2	4	370-460
sm015-2a	0° 57' 54.23" W	42° 27' 54.84" N	47.05	79.47	77.25	22.36	15.12	50	74.39	10.54	2	4	300-400
sm016-2a	0° 57' 53.96" W	42° 27' 54.87" N	50.05	174.21	74.43	15.10	34.89	63.5	82.07	8.02	2	4	370-460
sm018-2a	0° 57' 53.88" W	42° 27' 56.14" N	89.05	65.62	71.17	25.63	8.77	45.6	100.42	2.06	2	4	340-400
sm019-2a	0° 57' 53.84" W	42° 27' 56.4" N	93.55	253.84	72.85	352.77	26.67	61	129.21	4.027	2	4	340-400
sm020-2a	0° 57' 53.78" W	42° 27' 56.55" N	96.95	73.83	-48.18	145.06	-32.08	-51.2	85.61	8.74	2	4	300-400
sm021-1a	0° 57' 53.76" W	42° 27' 56.76" N	100.95	48.70	31.13	49.78	-33.64	13.8	48.13	11.23	2	4	* 300-400
sm022-1b	0° 57' 53.58" W	42° 27' 56.79" N	105.45	115.94	68.05	37.69	17.97	43.2	155.02	9.80	2	3	300-370
sm023-1b	0° 57' 53.51" W	42° 27' 57" N	111.25	6.51	62.20	10.95	-12.50	40.2	182.83	7.03	2	5	340-520
sm024-1b	0° 57' 53.44" W	42° 27' 57.12" N	115.75	240.99	66.40	355.50	30.38	63.6	110.65	11.31	2	3	300-370
sm025-1b	0° 57' 53.27" W	42° 27' 57.11" N	120.25	336.78	-39.64	241.01	-48.54	-40.1	27.60	29.2	2	4	* 300-400
sm026-2a	0° 57' 53.24" W	42° 27' 57.19" N	123.65	220.89	81.09	10.79	22.96	58.1	80.31	7.61	2	4	300-400
sm027-1b	0° 57' 53.11" W	42° 27' 57.42" N	127.95	299.99	80.69	5.79	12.41	53.5	140.17	9.07	2	4	300-400
sm028-1a	0° 57' 52.95" W	42° 27' 57.44" N	132.45	358.87	-16.65	276.75	-74.39	-33.2	198.36	9.49	2	5	* 370-520
sm029-1b	0° 57' 52.82" W	42° 27' 57.58" N	135.85	12.20	45.90	12.77	-29.04	30.8	231.70	4.02	2	4	300-400
sm031-1a	0° 58' 15.5640" W	42° 27' 24.2748" N	7.35	341.65	35.06	270.50	25.43	9.3	294.19	4.71	2	3	300-370
sm032-1a	0° 58' 15.5172" W	42° 27' 24.2388" N	8.85	284.25	29.01	278.38	-22.33	-1.7	389.88	2.58	2	3	300-370
sm033-2a	0° 58' 15.5388" W	42° 27' 24.1128" N	12.75	326.26	10.86	298.70	15.96	26.5	164.34	7.25	2	3	300-370
sm035-2a	0° 58' 15.7980" W	42° 27' 23.9328" N	19.3	338.97	10.47	298.07	28.44	30.8	194.74	5.25	2	4	300-400
sm037-1b	0° 58' 16.2300" W	42° 27' 23.5404" N	30.5	222.37	17.69	227.40	-72.16	-56.9	60.99	14.66	2	3	* 200-370
sm038-1a	0° 58' 16.1436" W	42° 27' 23.4108" N	32	2.77	0.42	309.31	52.76	49.6	444.55	2.85	2	5	490-560
sm039-1a	0° 58' 16.2228" W	42° 27' 23.5548" N	35	183.89	57.48	199.41	-25.74	-56.6	109.55	6.20	2	3	250-370
sm042-2a	0° 58' 17.2596" W	42° 27' 23.2056" N	50.2	265.34	49.57	251.22	-27.12	-23.4	313.08	13.73	2	6	640-670
sm043-1b	0° 58' 17.5620" W	42° 27' 23.0580" N	54.4	339.39	12.29	295.96	28.65	29.3	266.17	9.64	2	6	640-670
sm044-1b	0° 58' 17.8320" W	42° 27' 22.9932" N	56.8	310.29	-11.79	321.79	0.28	35.6	125.44	14.19	2	6	640-670
sm045-2a	0° 58' 18.1128" W	42° 27' 23.0256" N	60.5	1.35	-18.30	337.90	47.86	67.6	515.89	3.87	2	6	580-670
sm046-2a	0° 58' 18.3144" W	42° 27' 22.9536" N	64.1	190.33	54.65	200.65	-30.18	-58.4	1555.93	5.65	1	6	370-670
sm047-2b	0° 58' 18.6888" W	42° 27' 22.8672" N	68.6	187.24	56.03	199.97	-28.03	-57.5	1059.94	3.42	1	6	370-550
sm048-1a	0° 58' 18.9156" W	42° 27' 22.7988" N	70.1	143.22	42.51	173.28	-9.71	-52	465.70	5.16	2	6	460-580
sm049-1c	0° 58' 20.1180" W	42° 27' 22.5972" N	83.1	183.59	32.69	177.23	-42.64	-72.1	440.26	8.91	2	5	* 250-460
sm050-1b	0° 58' 20.2908" W	42° 27' 22.6188" N	84.6	204.32	11.92	167.99	-70.40	-75.6	468.81	4.42	2	6	* 300-580
sm051-2a	0° 58' 20.2800" W	42° 27' 22.5144" N	88.8	199.92	20.07	176.78	-61.91	-87.5	528.80	7.57	2	6	* 370-640
sm052-1a	0° 58' 20.5608" W	42° 27' 22.5108" N	90.8	355.52	-42.83	2.91	31.55	64.5	2362.25	2.30	2	6	550-670
sm053-2a	0° 58' 20.7552" W	42° 27' 22.5432" N	93.2	199.12	33.62	191.80	-51.08	-75.8	517.72	6.11	2	5	* 300-580
sm053-2a	0° 58' 20.7552" W	42° 27' 22.5432" N	93.2	347.14	-11.14	323.87	36.32	52.4	197.94	5.88	2	6	610-670
sm054-1a	0° 58' 20.8848" W	42° 27' 22.3200" N	97.4	216.07	37.56	214.91	-52.27	-61	260.23	8.13	2	6	* 340-580

sm055-1b	0° 58' 21.1512" W	42° 27' 22.2300" N	101.7	341.65	34.03	271.58	25.77	10.3	705.35	1.47	2	6	460-610
sm056-1a	0° 58' 21.2052" W	42° 27' 22.1256" N	105.9	176.67	29.58	169.60	-39.25	-68	516.01	12.25	2	5	* 300-550
sm057-2a	0° 58' 21.5184" W	42° 27' 22.0932" N	112	181.64	15.20	153.65	-49.18	-65.6	736.04	6.27	2	5	* 300-550
sm058-1a	0° 58' 21.9648" W	42° 27' 22.0212" N	113.8	233.03	44.76	232.81	-43.77	-43.9	349.45	6.48	2	5	* 370-580
sm058-1a	0° 58' 21.9648" W	42° 27' 22.0212" N	113.8	328.03	0.55	309.43	18.03	34.8	308.70	9.05	2	6	640-670
sm059-2a	0° 58' 22.0800" W	42° 27' 22.1472" N	116.8	191.71	7.98	146.47	-60.70	-65.3	483.97	7.56	2	6	* 400-610
sm060-1a	0° 58' 22.2024" W	42° 27' 21.9996" N	119.3	190.45	22.41	169.91	-53.53	-78.5	624.25	4.53	2	6	* 370-580
sm061-1b	0° 58' 22.3824" W	42° 27' 21.8340" N	125	299.10	-24.75	335.15	-9.88	37.5	2820.94	1.05	2	6	490-640
sm063-1b	0° 58' 22.5840" W	42° 27' 21.5496" N	129.7	180.41	-2.86	125.52	-50.32	-45.7	1995.80	1.86	1	6	300-590
sm064-2b	0° 58' 22.6596" W	42° 27' 21.3300" N	133.15	184.34	14.12	153.34	-51.99	-66.8	714.23	7.45	1	6	* 300-620
sm065-2b	0° 58' 22.6884" W	42° 27' 21.2724" N	135.65	179.33	4.64	137.09	-49.11	-53.7	1220.04	4.36	1	6	* 300-620
sm066-1a	0° 58' 22.9188" W	42° 27' 20.9808" N	140.25	180.63	7.75	142.10	-49.99	-57.7	1840.01	10.49	2	6	* 300-590
sm067-2a	0° 58' 22.9368" W	42° 27' 20.6820" N	147.75	175.95	4.76	136.83	-45.75	-51.9	1224.55	9.41	2	6	* 300-620 (390out)
sm068-1c	0° 58' 22.9548" W	42° 27' 20.5560" N	150	182.63	3.28	135.40	-52.51	-54	2082.25	2.17	1	6	400-620
sm069-2a	0° 58' 22.9800" W	42° 27' 20.3076" N	156.3	257.23	36.88	258.88	-39.56	-22.9	157.35	13.78	2	5	* 400-560
sm070-1a	0° 58' 23.0736" W	42° 27' 20.0664" N	158.3	172.65	0.90	131.22	-42.64	-46.4	2429.36	2.06	1	6	400-620
sm071-1b	0° 58' 22.9764" W	42° 27' 19.9944" N	161.3	174.35	7.06	139.82	-43.92	-53.2	1458.52	3.89	1	6	350-620
sm072-2a	0° 58' 22.8180" W	42° 27' 19.7784" N	164.3	182.41	7.76	142.59	-51.73	-58.9	891.82	2.02	2	6	470-620
sm073-2a	0° 58' 22.8792" W	42° 27' 19.4868" N	166.3	133.79	66.22	196.27	-1.53	-45.8	643.83	4.30	2	5	300-560
sm074-2a	0° 58' 22.7352" W	42° 27' 19.1808" N	172.3	148.07	-22.61	106.34	-16.64	-17.8	2048.38	2.80	2	6	470-620
sm075-2a	0° 58' 21.9720" W	42° 27' 18.3096" N	178.1	180.98	48.17	192.68	-10.72	-51.3	184.19	10.64	2	6	* 300-590
sm076-2b	0° 58' 21.3240" W	42° 27' 17.8488" N	181.3	196.22	2.98	179.26	-56.61	-84.7	416.75	2.62	2	5	500-560
sm078-1a	0° 58' 20.0064" W	42° 27' 16.9812" N	189.9	185.52	-3.75	157.09	-54.58	-70.8	999.03	4.03	1	6	440-650
sm079-1a	0° 58' 19.7040" W	42° 27' 16.4592" N	193.1	69.34	79.90	208.21	33.18	-24.1	704.52	16.20	2	6	* 400-650
sm080-1b	0° 58' 19.4628" W	42° 27' 16.0812" N	196.8	163.12	22.70	164.12	-20.67	-55.3	204.79	5.95	2	6	500-620
sm081-1b	0° 58' 18.9120" W	42° 27' 15.6240" N	201	179.61	11.64	167.53	-39.67	-67.5	1637.55	2.26	1	6	440-620
sm082-1b	0° 58' 18.4476" W	42° 27' 15.4188" N	204.8	297.33	31.61	273.21	6.81	4.7	1798.79	1.68	2	6	400-590
sm083-2b	0° 58' 17.7024" W	42° 27' 14.9400" N	209.1	170.27	37.80	179.95	-14.46	-54.9	324.83	16.90	2	6	* 300-620
sm084-2a	0° 58' 17.2380" W	42° 27' 14.4828" N	213.4	167.25	-9.83	134.74	-42.26	-48.8	2108.59	1.99	1	6	400-620
sm086-1b	0° 58' 16.1292" W	42° 27' 13.6044" N	222	195.65	24.49	192.79	-37.09	-65.7	530.95	4.33	2	6	470-590
sm087-1b	0° 58' 15.6576" W	42° 27' 13.2696" N	226	178.54	-37.12	94.78	-56.75	-27.3	1301.22	1.59	2	6	400-620
sm088-2c	0° 58' 15.0456" W	42° 27' 12.7836" N	230.5	163.21	-6.33	136.57	-37.14	-47.7	1431.00	4.85	2	6	* 400-590
sm089-2a	0° 58' 14.3580" W	42° 27' 12.3984" N	235.4	331.68	29.74	284.84	34.27	23.4	524.13	3.35	2	6	620-650
sm091-2a	0° 58' 13.9440" W	42° 27' 11.9016" N	241.7	37.42	-43.14	36.90	21.83	45.3	260.01	5.18	2	6	530-560
sm092-1a	0° 58' 13.6020" W	42° 27' 11.6856" N	246.6	322.79	15.28	297.91	22.24	28.3	2169.16	2.38	2	6	560-650
sm093-2b	0° 58' 13.3500" W	42° 27' 11.3724" N	250.6	358.87	8.79	323.84	52.00	59.9	136.48	16.76	2	5	500-560
sm095-1a	0° 58' 13.7532" W	42° 27' 11.2608" N	256.6	339.99	-18.71	338.84	20.90	53.4	421.25	4.97	2	6	620-670
sm097-1b	0° 58' 14.7180" W	42° 27' 11.2860" N	262.9	337.29	-18.60	337.12	18.91	51.6	249.27	7.78	2	6	620-670
sm099-1b	0° 58' 15.3084" W	42° 27' 11.4120" N	267.4	343.04	16.20	304.79	40.85	40.9	224.27	7.24	2	6	620-670
sm101-2b	0° 58' 15.9600" W	42° 27' 11.4336" N	272.75	288.42	-44.32	345.31	-4.71	43.3	1290.18	2.17	2	6	620-670
sm103-1a	0° 58' 17.4864" W	42° 27' 11.4444" N	280.25	313.08	-41.12	341.11	13.13	50.5	925.34	3.83	2	6	620-670
sm105-1b	0° 58' 16.8168" W	42° 27' 8.8308" N	329.75	170.81	12.73	133.99	-50.56	-52	914.56	3.27	1	6	490-670
sm109-1a	0° 58' 15.8232" W	42° 27' 7.4052" N	351.55	201.43	44.18	200.41	-50.10	-70	244.53	5.49	1	6	530-670
sm112-2b	0° 58' 14.3076" W	42° 27' 6.1992" N	369.35	178.66	82.59	206.08	-11.31	-46.6	183.37	5.05	2	6	590-670(620out)
sm114-2b	0° 58' 12.9432" W	42° 27' 4.7520" N	385.05	159.43	21.20	143.20	-38.42	-52.9	541.83	4.58	2	6	300-670
sm117-2a	0° 58' 12.2340" W	42° 27' 3.4740" N	402.45	155.52	45.19	165.16	-30.19	-60.9	112.04	11.90	2	6	* 400-590
sm119-1a	0° 58' 12.1620" W	42° 27' 2.5524" N	421.45	158.86	63.98	182.19	-19.29	-57.4	704.36	4.53	1	6	350-650

sm121-1b	0° 58' 12.2160" W	42° 27' 1.9800" N	437.45	232.53	50.69	223.77	-32.29	-45.4	1626.05	3.74	1	6	350-670
sm123-2a	0° 58' 12.5436" W	42° 27' 1.7640" N	445.35	123.05	67.33	177.86	-4.99	-50	433.05	9.95	2	6	* 530-670
sm125-2a	0° 58' 13.3824" W	42° 27' 1.6020" N	450.35	190.59	42.44	189.87	-46.72	-73.5	440.65	8.30	2	6	* 450-650
sm127-2a	0° 58' 13.5840" W	42° 27' 1.5444" N	458.75	153.58	51.61	170.14	-25.35	-59.7	2119.95	3.69	2	6	400-670
sm129-1b	0° 58' 13.9332" W	42° 27' 0.8928" N	475.25	155.16	48.87	168.38	-27.80	-60.6	1879.90	3.36	2	6	400-670(620out)
sm131-2a	0° 58' 13.9728" W	42° 27' 0.3672" N	487.95	205.57	51.42	204.43	-38.36	-60.8	225.64	3.42	1	6	450-670(560out)
sm133-2b	0° 58' 14.2068" W	42° 26' 59.9208" N	499.45	165.15	47.55	172.41	-33.63	-65.1	1012.73	2.38	1	6	250-670(560out)
sm135-2b	0° 58' 14.0124" W	42° 26' 59.0964" N	509.45	195.41	31.73	192.63	-57.97	-79.7	563.53	3.61	1	6	350-670
sm137-1b	0° 58' 13.9332" W	42° 26' 58.4160" N	524.75	323.47	52.57	232.56	19.58	-18.9	403.84	2.45	2	6	530-620
sm139-2a	0° 58' 13.3824" W	42° 26' 57.7104" N	538.05	77.09	62.41	176.32	14.57	-40	749.73	4.41	2	6	450-670
sm141-2b	0° 58' 13.6920" W	42° 26' 56.8536" N	553.35	137.11	55.79	168.82	-14.85	-53.7	304.60	7.40	2	6	490-650
sm143-1a	0° 58' 13.7748" W	42° 26' 56.3892" N	566.65	188.65	36.64	185.18	-51.88	-79.2	441.94	5.66	2	6	450-670(490out)
sm145-1a	0° 58' 13.8828" W	42° 26' 56.2740" N	576.25	171.27	44.94	174.28	-38.37	-68.6	540.86	3.73	2	6	530-670
sm147-2a	0° 58' 14.5560" W	42° 26' 55.8060" N	588.25	219.30	66.92	208.02	-21.72	-50.4	110.54	9.27	2	6	560-670
sm149-2a	0° 58' 14.9736" W	42° 26' 55.7232" N	596.45	134.77	75.24	186.55	-6.13	-50.2	538.15	4.88	2	6	490-670
sm151-1a	0° 58' 15.8160" W	42° 26' 55.2732" N	611.05	289.58	-57.26	347.26	-0.23	45.9	784.98	1.05	2	4	350-450
sm155-2a	0° 58' 17.1660" W	42° 26' 54.3408" N	643.25	325.21	-17.96	311.63	33.27	42.5	123.76	9.10	2	5	560-620
sm157-2a	0° 58' 17.5440" W	42° 26' 54.1428" N	649.55	189.69	47.64	190.73	-41.52	-69.4	1811.84	2.06	1	6	300-590
sm159-2b	0° 58' 18.1092" W	42° 26' 53.9304" N	655.85	161.28	-71.87	31.58	-14.05	32.7	1705.60	2.29	2	6	350-620
sm161-1a	0° 58' 19.0740" W	42° 26' 53.9736" N	663.35	227.75	60.67	214.66	-25.69	-48.4	73.81	8.37	2	5	350-530(450out)
sm163-1a	0° 58' 19.5780" W	42° 26' 53.8260" N	670.25	328.80	-24.10	319.86	34.89	49	83.77	13.49	2	5	530-590
sm165-2a	0° 58' 20.3016" W	42° 26' 53.2464" N	682.25	45.47	-48.59	40.77	36.66	49.4	274.79	3.56	2	5	590-620
sm167-1b	0° 58' 20.6184" W	42° 26' 52.6560" N	697.05	301.76	-50.17	340.77	7.50	47.7	125.15	6.30	2	6	620-670
sm169-1a	0° 58' 20.7660" W	42° 26' 52.3860" N	705.25	79.59	-60.81	45.72	14.29	36.6	133.88	6.77	2	6	560-670
sm171-1b	0° 58' 20.8848" W	42° 26' 51.8568" N	719.35	236.14	70.16	212.01	-15.91	-45.6	55.51	6.26	2	6	560-650
sm173-2a	0° 58' 20.9928" W	42° 26' 50.9748" N	735.85	196.57	39.12	195.79	-50.76	-73.3	251.79	10.74	2	6	450-670
sm175-2a	0° 58' 20.4672" W	42° 26' 50.1216" N	756.15	124.66	75.49	185.94	-3.64	-49	168.28	10.22	2	6	400-670
sm177-2a	0° 58' 20.0460" W	42° 26' 49.4628" N	772.85	285.05	26.23	263.68	-4.44	-6.2	412.29	2.76	2	5	200-530
sm030-2a	0° 58' 15.2940" W	42° 27' 24.3396" N	0	56.12	71.10	214.57	18.13	-29.4	92.86	18.42	3	4	* 300-400
sm034-2b	0° 58' 15.6648" W	42° 27' 23.8932" N	15	313.94	-19.07	329.11	3.72	40.9	75.76	13.30	3	3	* 250-370
sm040-2a	0° 58' 16.4748" W	42° 27' 23.4360" N	39.5	307.59	5.26	304.74	-2.40	24	892.11	2.99	3	6	640-670
sm041-1b	0° 58' 16.7124" W	42° 27' 23.1732" N	44.2	272.58	82.63	225.87	-4.47	-32.7	490.59	2.78	3	5	370-580
sm051-2a	0° 58' 20.2800" W	42° 27' 22.5144" N	88.8	309.47	3.05	306.95	-0.53	26.1	634.50	8.05	3	6	640-670
sm054-1a	0° 58' 20.8848" W	42° 27' 22.3200" N	97.4	330.62	52.30	255.88	12.44	-6	124.77	6.20	3	6	640-670
sm056-1a	0° 58' 21.2052" W	42° 27' 22.1256" N	105.9	293.89	10.64	298.94	-15.83	15	726.18	0.46	3	6	640-670
sm088-2c	0° 58' 15.0456" W	42° 27' 12.7836" N	230.5	331.42	-38.39	350.33	3.07	48.2	321.43	2.43	3	6	650-670
sm089-2a	0° 58' 14.3580" W	42° 27' 12.3984" N	235.4	142.64	51.26	177.85	9.08	-42.9	281.35	12.58	3	6	* 400-590
sm107-2b	0° 58' 15.9960" W	42° 27' 7.9308" N	341.25	59.14	80.30	205.28	3.48	-40.3	58.89	1.11	3	6	560-620(590out)
sm153-1b	0° 58' 16.4532" W	42° 26' 54.7008" N	630.55	59.87	1.17	111.83	50.11	6.4	115.81	6.67	3	6	620-650

Graphical abstract

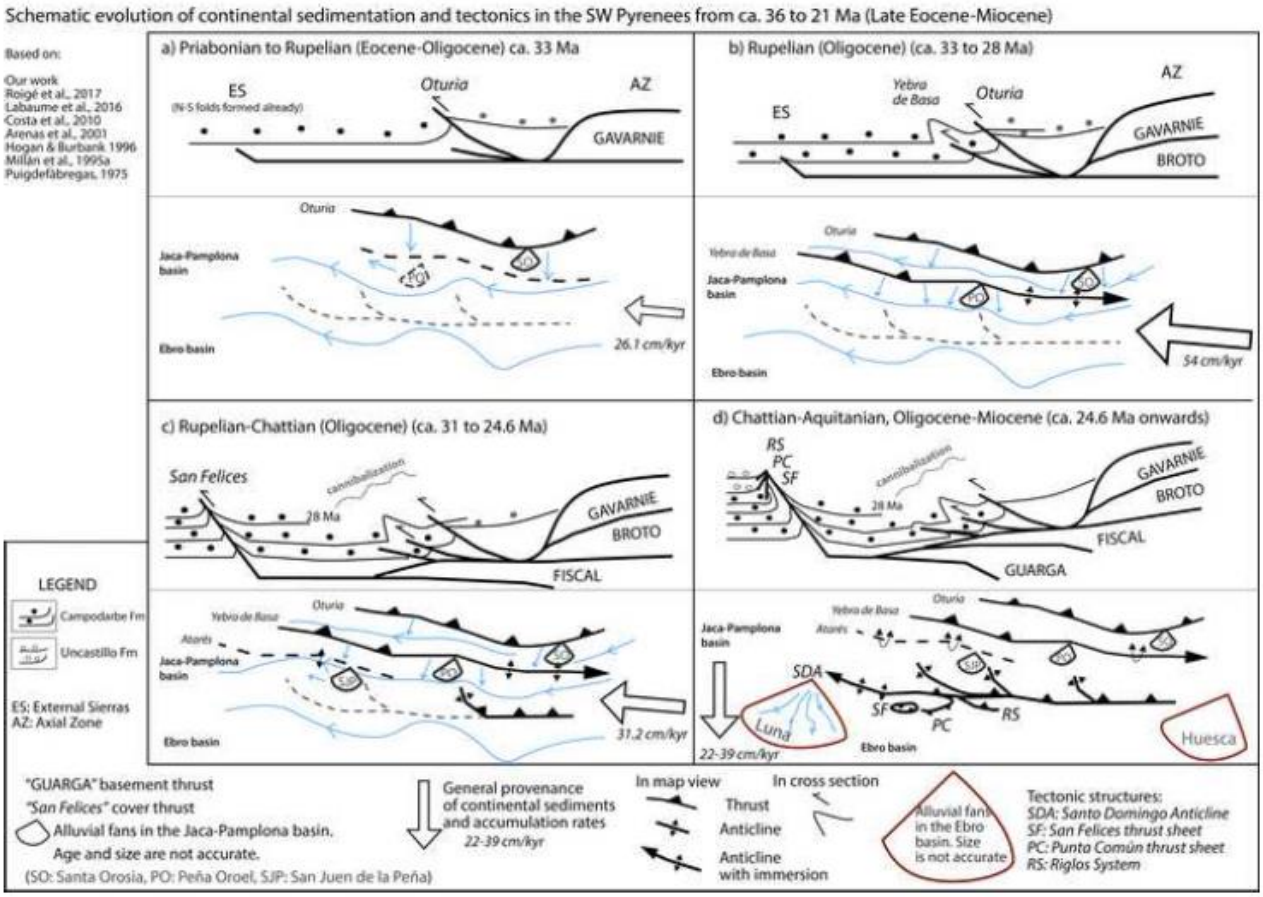

Highlights

- Bracketing the timing of the deformation in the southern margin of the Pyrenees from 31.3 to 24.55 Ma Rupelian-Chattian (Oligocene, Gavarnie nappe), and from 24.55 to 21.2 Ma (Chattian-Aquitanian, Oligocene-Miocene, Guarga thrust).
- Deformation for the latest Pyrenean front (syn-Guarga thrust) is younger than previously assigned.
- Accumulation rates vary from ~22 to ~39 cm/kyr between the genetic stratigraphic units in the alluvial Uncastillo Fm
- Accumulation rates vary from ~26 to ~55 cm/kyr in the underlying fuvial Campodarbe Fm (average of ~36 cm/kyr).